DALTON
FULL PAPER

Redox-induced κ^2–κ^3 isomerisation in hydrotris(pyrazolyl)-boratorhodium complexes: synthesis, structure and ESR spectroscopy of stabilised rhodium(II) species

Neil G. Connelly,*[a] David J. H. Emslie,[a] William E. Geiger,[b] Owen D. Hayward,[a] Emma B. Linehan,[a] A. Guy Orpen,[a] Michael J. Quayle[a] and Philip H. Rieger[c]

[a] *School of Chemistry, University of Bristol, Bristol, UK BS8 1TS*
[b] *Department of Chemistry, University of Vermont, Burlington, VT 05405, USA*
[c] *Department of Chemistry, Brown University, Rhode Island, RI 02912, USA*

Received 9th October 2000, Accepted 22nd December 2000
First published as an Advance Article on the web 14th February 2001

The complexes [Rh(CO)LTp′] {Tp′ = HBR_3, R = 3,5-dimethylpyrazolyl; L = PPh_3 **2**, PCy_3 **3**, L = $P(NMe_2)_3$ **4**, $P(C_6H_4Me\text{-}p)_3$ **5** or $P(C_6H_4Me\text{-}m)_3$ **6**}, prepared from $[Rh(CO)_2Tp']$ **1** and L, and $[Rh(PPh_3)_2L']$ [L′ = Tp′ **8**, Tp **9** or $B(pz)_4$ **10** {Tp = $HB(pz)_3$, pz = pyrazolyl}] and [Rh(dppe)Tp′] **11**, prepared from $[\{Rh(\mu\text{-}Cl)(PPh_3)_2\}_2]$ or $[\{Rh(\mu\text{-}Cl)(dppe)\}_2]$ and KL′, adopt four-co-ordinate κ^2 structures, confirmed in the cases of **2**–**4**, **6** and **8** by X-ray structural studies. By contrast, complex [Rh(CO){$P(OPh)_3$}Tp′] **7** has a distorted five-co-ordinate square pyramidal structure with a long Rh · · · N contact [2.764(2) Å] in the apical site and an essentially planar $Rh(CO)PN_2$ basal plane. Each complex undergoes fluxional processes on the NMR timescale. One-electron oxidation of **1**–**11** gives the κ^3 rhodium(II) cations $\mathbf{1}^+$–$\mathbf{11}^+$; the crystal structures of salts of $\mathbf{2}^+$ and $\mathbf{8}^+$ confirm stabilisation of the unusual rhodium(II) oxidation state by axial co-ordination of the third pyrazolyl ring as a result of oxidatively induced κ^2–κ^3 isomerisation. These structures and ESR spectroscopy are consistent with a five-co-ordinate square pyramidal geometry with the unpaired electron in a σ^* $Rh\text{–}N_{axial}$ orbital.

Introduction

Rhodium(I) hydrotris(pyrazolyl)borate complexes such as $[RhL_2(HBR_3)]$ (L = CO, L_2 = η^4-diene, *etc*.; R = pyrazolyl) exist in one or more of three forms, namely two square planar, 16-electron isomers $[RhL_2(\kappa^2\text{-}HBR_3)]$ and a five-co-ordinate, 18-electron isomer $[RhL_2(\kappa^3\text{-}HBR_3)]$ (**A**–**C**, Scheme 1); the

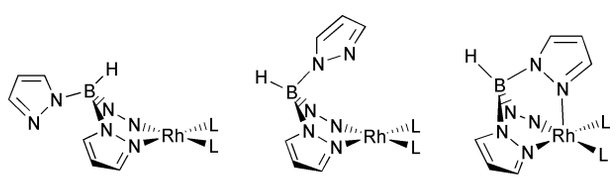

(**A**) (**B**) (**C**)

Scheme 1

relative abundance of the three forms depends on R and L and, in solution, on the solvent.[1–4] The interconversion of κ^2 and κ^3 rhodium(I) complexes such as $[Rh(CO)_2(\kappa^2\text{-}HBR_3)]$ and $[Rh(CO)_2(\kappa^3\text{-}HBR_3)]$ is particularly important in photo-induced C–H activation reactions with both aromatic and saturated hydrocarbons[5–8] which can give six-co-ordinate rhodium(III) hydrido alkyl or aryl complexes, for example $[RhHPh(CO)(\kappa^3\text{-}HBR_3)]$ with benzene.

We have previously noted[9] that the rhodium(I) complex $[Rh(CO)(PPh_3)(\kappa^2\text{-}Tp')]$ (Tp′ = HBR_3, R = 3,5-dimethylpyrazolyl) also undergoes *redox-induced* isomerisation, one-electron oxidation giving $[Rh(CO)(PPh_3)(\kappa^3\text{-}Tp')]^+$ in which the unusual rhodium(II) oxidation state is stabilised by *N*-co-ordination of the third pyrazolyl ring. We now give details of the synthesis, structure and electrochemistry of a wider range of complexes $[RhL_2Tp']$ and their chemical oxidation to stable rhodium(II) cations which have been fully characterised both structurally and by ESR spectroscopy.

Results and discussion

Two series of complexes, namely $[Rh(CO)(PR_3)Tp']$ and $[RhL_2Tp']$ (L = monodentate *P*-donor ligand, L_2 = dppe = $Ph_2PCH_2CH_2PPh_2$), have been studied here. Several other such species have been prepared[6,10] (mostly since our preliminary communication regarding the oxidation of $[Rh(CO)(PPh_3)Tp']$[9]) including $[Rh(CO)(PMe_3)Tp']$,[11] $[Rh(PMe_3)_2Tp']$,[12] [Rh(CO)(PMePh$_2$)L′] {L′ = hydrotris(4-chloro-3,5-dimethylpyrazolyl)borate},[13] $[Rh(PPh_3)_2Tp]$ {Tp = hydrotris(pyrazolyl)borate}[14] and $[RhL_2L']$ {L_2 = *cis*-1,2-bis(diphenylphosphino)ethene, L′ = hydrotris(3,5-diisopropylpyrazolyl)borate}.[15] We have extended these series considerably in order to have a wider range of species available for comparative electrochemical and structural studies.

The preparation of $[Rh(CO)LTp']$ and $[RhL_2Tp']$

Heating an *n*-hexane solution of $[Rh(CO)_2Tp']$ **1** with PPh_3 or PCy_3 under reflux gave $[Rh(CO)LTp']$ (L = PPh_3 **2** or PCy_3 **3**) after 24 and 4 h respectively but in the presence of Me_3NO the reaction with PPh_3 is complete after 4 h at room temperature; the analogous complexes $[Rh(CO)LTp']$ {L = $P(NMe_2)_3$ **4**, $P(C_6H_4Me\text{-}p)_3$ **5**, $P(C_6H_4Me\text{-}m)_3$ **6** or $P(OPh)_3$ **7**} were prepared in toluene from **1** and $P(NMe_2)_3$, $P(C_6H_4Me\text{-}p)_3$, $P(C_6H_4Me\text{-}m)_3$ (at room temperature) or $P(OPh)_3$ (at 50 °C). The bis(phosphine) complexes $[Rh(PPh_3)_2L']$ {L′ = Tp′ **8**, Tp **9**[14] or $B(pz)_4$ **10** (pz = pyrazolyl)} and the ditertiary phosphine derivative [Rh(dppe)Tp′] **11** were synthesized by treating $[\{Rh(\mu\text{-}Cl)(PPh_3)_2\}_2]$ or $[\{Rh(\mu\text{-}Cl)(dppe)\}_2]$ with KL′ in thf at room temperature.

Complexes **2**–**11** were characterised by elemental analysis, IR spectroscopy, cyclic voltammetry (Table 1) and ^1H, $^{13}C\text{-}\{^1H\}$ and ^{31}P NMR spectroscopy (Table 2). In addition, the molecular structures of **2**–**4** and **6**–**8** have been determined by X-ray crystallography.

The CO and BH stretches in the IR spectra of $[Rh(CO)_2$-

 DOI: 10.1039/b008131k

Table 1 Analytical data for rhodium hydrotris(pyrazolyl)borate complexes[a]

Complex	Colour	Yield (%)	Analysis (%)[b]			IR[c]/cm^{-1}					
			C	H	N	ν(CO)	ν(CO)[d]	ν(BH)	ν(BH)[d]	$E^{\circ\prime}$/V[c,e]	λ_{max}[f]/nm
2 [Rh(CO)(PPh_3)Tp′]	Bright yellow	67	59.2 (58.8)	5.4 (5.7)	11.9 (12.2)	1978	1975, 1969, 1965[g]	2473	2466	−0.16[h]	
3 [Rh(CO)(PCy_3)Tp′]	Pale yellow	42	57.8 (57.6)	8.5 (7.8)	11.6 (11.9)	1966	1968	2475	2459	0.20	
4 [Rh(CO){$P(NMe_2)_3$}Tp′]	Yellow	64	45.1 (44.7)	6.9 (6.8)	21.1 (21.3)	1975	1979	2474	2466	−0.36	
5 [Rh(CO){$P(C_6H_4Me\text{-}p)_3$}Tp′]	Bright yellow	43	60.2 (60.7)	6.1 (5.9)	11.4 (11.5)	1976	1977	2473	2493	−0.30	
6 [Rh(CO){$P(C_6H_4Me\text{-}m)_3$}Tp′]	Green-yellow	45	60.6 (60.7)	6.1 (5.9)	11.6 (11.5)	1975	1969	2473	2486	−0.28	
7 [Rh(CO){$P(OPh)_3$}Tp′]	Yellow-orange	32	55.6 (55.3)	5.2 (5.1)	11.3 (11.4)	2007br	1984	2520, 2479	2519	−0.17	
8 [Rh(PPh_3)$_2$Tp′]	Yellow	48	66.5 (66.3)	5.7 (5.7)	9.1 (9.1)	—	—	2467	2466	−0.61	
9 [Rh(PPh_3)$_2$Tp]	Yellow	73	64.4 (64.3)	4.9 (4.8)	10.3 (10.0)	—	—	—	2414w, 2394s	—	
10 [Rh(PPh_3)$_2${B(pz)$_4$}]	Yellow	44	62.9 (63.6)	4.4 (4.7)	12.8 (12.4)	—	—	—	—	—	
11 [Rh(dppe)Tp′]	Yellow	40	61.8 (61.7)	5.9 (5.8)	10.3 (10.5)	—	—	2472	2468	−0.77	
[Rh(CO)(PPh_3)Tp′][PF_6]·CH_2Cl_2 **2**$^+$ [PF_6]$^-$·CH_2Cl_2	Dark green	72	45.6 (45.7)	4.1 (4.3)	9.2 (9.1)	2070	2063	2558	2562	−0.26	391(950), 595(380), 759(140)
[Rh(CO){$P(NMe_2)_3$}Tp′][PF_6] **4**$^+$[PF_6]$^-$	Purple	64	36.2 (35.9)	5.6 (5.5)	17.1 (17.1)	2063	2060, 2051[g]	2558	2558	−0.38	404(640), 502(610), *ca.* 750(sh)
[Rh(CO){$P(C_6H_4Me\text{-}p)_3$}Tp′][PF_6]·0.7 CH_2Cl_2 **5**$^+$ [PF_6]$^-$·0.7 CH_2Cl_2	Dark green	53	48.2 (48.3)	5.1 (4.8)	9.3 (9.0)	2069	2060	2558	—	−0.28	592, 756
[Rh(CO){$P(C_6H_4Me\text{-}m)_3$}Tp′][PF_6]·0.5 CH_2Cl_2 **6**$^+$ [PF_6]$^-$·0.5 CH_2Cl_2	Grey-green	43	49.1 (49.0)	4.6 (4.8)	8.9 (9.1)	2069	2059	2557	—	−0.28	592, 754
[Rh(PPh_3)$_2$Tp′][BF_4] **8**$^+$ [BF_4]$^-$	Purple	66	60.5 (60.5)	5.2 (5.2)	8.0 (8.4)	—	—	2556	2551	−0.63	523(350), 753(130)
[Rh(PPh_3)$_2$Tp′][PF_6] **8**$^+$ [PF_6]$^-$	Purple	83	56.9 (57.3)	4.3 (4.9)	7.3 (7.9)	—	—	2556	2555	—	—
[Rh(PPh_3)$_2$Tp][PF_6]·0.5 CH_2Cl_2 **9**$^+$ [PF_6]$^-$·0.5 CH_2Cl_2	Pale purple	75	53.4 (53.2)	4.1 (4.0)	8.4 (8.2)	—	—	—	—	—	—
[Rh(dppe)Tp′][PF_6] **11**$^+$ [PF_6]$^-$	Olive green	69	52.7 (52.2)	4.8 (4.9)	8.8 (8.9)	—	—	2557	—	−0.77	—
12 [Rh(CO)(PPh_3)(HTp′)][BF_4]	Pale yellow	60	52.5 (52.5)	4.8 (4.9)	10.8 (10.8)	1990	1983	2511	2497	—	—

[a] Tp = Hydrotris(pyrazolyl)borate; Tp′ = hydrotris(3,5-dimethylpyrazolylborate. [b] Calculated values in parentheses. [c] In CH_2Cl_2 unless stated otherwise. [d] In Nujol. [e] Potential, *vs.* the $[Fe(\eta\text{-}C_5H_5)_2]^+$–$[Fe(\eta\text{-}C_5H_5)_2]$ couple at 0.0 V, for oxidation of the neutral rhodium(I) complexes or of reduction of the cationic rhodium(II) complexes, at a glassy carbon electrode. [f] In CH_2Cl_2; absorption coefficient, ε/dm^3 mol^{-1} cm^{-1} in parentheses. [g] Additional bands due to solid state splitting. [h] In thf.

Table 2 Proton, ^{13}C-{^{1}H} and ^{31}P NMR spectroscopic data for rhodium hydrotris(pyrazolyl)borate complexes[a]

Complex	^{1}H	^{13}C-{^{1}H}	^{31}P
1 [Rh(CO)$_2$Tp′]	[b]	190.30 {d, $J_{C,Rh}$ 77, CO}, 150.19 (s, *C*CH$_3$), 145.20 (s, *C*CH$_3$), 106.20 (s, CH), 15.35 (s, CH$_3$), 12.80 (s, CH$_3$)	
2 [Rh(CO)(PPh$_3$)Tp′]	7.8–7.25 {m, 15H, P(C$_6$H$_5$)$_3$}, 5.65 (s, 3H, Pz CH), 2.16 (s, 9H, CH$_3$), 1.81 (s, 9H, CH$_3$)	190.25 {dd, $J_{C,Rh}$ 70, $J_{C,P}$ 23, CO}, 149.48 (d, J 1, *C*CH$_3$), 145.71 (s, *C*CH$_3$), 134.79 {dd, $J_{C,P}$ 12, J 1, P(C$_6$H$_5$)$_3$}, 133.71 {d, $J_{C,P}$ 48, P(C$_6$H$_5$)$_3$}, 130.34 {d, $J_{C,P}$ 2, P(C$_6$H$_5$)$_3$}, 128.36 {d, $J_{C,P}$ 11, P(C$_6$H$_5$)$_3$}, 106.35 (s, pz CH), 14.81 (s, (CH$_3$), 12.92 (s, CH$_3$)	42.22 (d, $J_{P,Rh}$ 162)
3 [Rh(CO)(PCy$_3$)Tp′]	5.89 (s, 1H, pz CH), 5.75 (s, 2H, pz CH), 2.43 (s, 3H, CH$_3$), 2.27 (s, 3H, CH$_3$), 2.21 (s, 6H, CH$_3$), 2.1–0.9 {m, CH$_3$ and P(C$_6$H$_{11}$)$_3$}[c]	190.54 (dd, $J_{C,Rh}$ 74, $J_{C,P}$ 22, CO), 149.44 (s, *C*CH$_3$), 148.73 (s, *C*CH$_3$), 148.44 (s, *C*CH$_3$), 147.10 (s, *C*CH$_3$), 146.21 (s, *C*CH$_3$), 142.91 (s, *C*CH$_3$), 106.19 (s, pz *C*H), 105.69 (s, pz *C*H), 31.9–10.9 {m, *C*H$_3$ and P(C$_6$H$_{11}$)$_3$}[d]	47.50 (d, $J_{P,Rh}$ 152)
	5.93 (s, 1H, pzCH), 5.85 (s, 1H, pzCH), 5.76 (s, 1H, pz CH), 2.44 (s, 3H, CH$_3$), 2.39 (s, 3H, CH$_3$), 2.34 (s, 3H, CH$_3$), 2.28 (s, 3H, CH$_3$), 2.12 (s, 3H, CH$_3$), 2.0–0.8 {m, CH$_3$ and P(C$_6$H$_{11}$)$_3$}[d]		
4 [Rh(CO){P(NMe$_2$)$_3$}Tp′]	5.77 (s, 3H, CH), 2.46 [d, 18H, $J_{H,P}$ 10, P{N(CH$_3$)$_2$}$_3$], 2.24 (s, 9H, pz CH$_3$), 2.11 (s, 9H, pz CH$_3$)	189.77 {dd, $J_{C,Rh}$ 74, $J_{C,P}$ 26, CO}, 149.37 (s, *C*CH$_3$), 145.55 (s, *C*CH$_3$), 106.24 (s, CH), 38.44 [d, $J_{C,P}$ 7, P{N(CH$_3$)$_2$}$_3$], 14.90 (s, pz CH$_3$), 12.93 (s, pz CH$_3$)	123.73 (d, $J_{P,Rh}$ 206)
5 [Rh(CO){P(C$_6$H$_4$Me-*p*)$_3$}Tp′]	7.38–7.28 {m, 6H, P(C$_6$*H*$_4$CH$_3$)$_3$}, 7.13–7.06 {m, 6H, P(C$_6$*H*$_4$CH$_3$)$_3$}, 5.65 (s, 3H, pz CH), 2.34 {s, 9H, P(C$_6$H$_4$C*H*$_3$)$_3$}, 2.15 (s, 9H, pz CH$_3$), 1.83 (s, 9H, pz CH$_3$)	190.40 {dd, $J_{C,Rh}$ 71, $J_{C,P}$ 23, CO}, 149.46 (s, pz *C*CH$_3$), 145.61 (s, pz *C*CH$_3$), 140.51 {d, $J_{C,P}$ 2, P(*C*$_6$H$_4$CH$_3$)$_3$}, 134.62 {d, $J_{C,P}$ 11, P(*C*$_6$H$_4$CH$_3$)$_3$}, 130.79 {d, $J_{C,P}$ 51, P(*C*$_6$H$_4$CH$_3$)$_3$}, 129.01 {d, $J_{C,P}$ 11, P(*C*$_6$H$_4$CH$_3$)$_3$}, 106.30 (s, pz CH), 21.43 {d, J 1, P(C$_6$H$_4$*C*H$_3$)$_3$}, 14.84 (s, pz CH$_3$), 12.93 (s, pz CH$_3$)	39.50 (d, $J_{P,Rh}$ 160)
6 [Rh(CO){P(C$_6$H$_4$Me-*m*)$_3$}Tp′]	7.39 {d, 3H, $J_{H,P}$ 12, P(C$_6$*H*$_4$CH$_3$)$_3$}, 7.4–7.1 {m, 9H, P(C$_6$*H*$_4$CH$_3$)$_3$}, 5.62 (s, 3H, pz CH), 2.26 {s, 9H, P(C$_6$H$_4$C*H*$_3$)$_3$}, 2.15 (s, 9H, pz CH$_3$), 1.81 (s, 9H, pz CH$_3$)	190.48 {dd, $J_{C,Rh}$ 70, $J_{C,P}$ 24, CO}, 149.42 (s, pz *C*CH$_3$), 145.59 (s, pz *C*CH$_3$), 138.12 {d, $J_{C,P}$ 10, P(*C*$_6$H$_4$CH$_3$)$_3$}, 135.84 {d, $J_{C,P}$ 13, P(*C*$_6$H$_4$CH$_3$)$_3$}, 133.50 {d, $J_{C,P}$ 48, P(*C*$_6$H$_4$CH$_3$)$_3$}, 131.42 {d, $J_{C,P}$ 9, P(*C*$_6$H$_4$CH$_3$)$_3$}, 130.99 {d, $J_{C,P}$ 3, P(*C*$_6$H$_4$CH$_3$)$_3$}, 128.94 {d, $J_{C,P}$ 10, P(*C*$_6$H$_4$CH$_3$)$_3$}, 106.15 (s, pz CH), 21.49 {s, P(C$_6$H$_4$*C*H$_3$)$_3$}, 14.73 (s, pz C*C*H$_3$), 12.85 (s, pz C*C*H$_3$)	42.01 (d, $J_{P,Rh}$ 161)
7 [Rh(CO){P(OPh)$_3$}Tp′]	7.38–7.06 {m, 15H, P(OC$_6$H$_5$)$_3$}, 5.72 (s, 3H, pz CH), 2.25 (s, 9H, CH$_3$), 2.22 (s, 9H, CH$_3$)	189.02 {dd, $J_{C,Rh}$ 69, $J_{C,P}$ 27, CO}, 151.36 {d, $J_{C,P}$ 7, P(OC$_6$H$_5$)$_3$}, 149.69 (dd, $J_{C,P}$ 2, $J_{C,Rh}$ 2, *C*CH$_3$), 145.55 (s, C*C*H$_3$), 129.78 {s, P(OC$_6$H$_5$)$_3$}, 124.94 {s, P(OC$_6$H$_5$)$_3$}, 121.126 {d, $J_{C,P}$ 6, P(O*C*$_6$H$_5$)$_3$}, 106.07 (s, pz CH), 15.11 (s, CH$_3$), 13.01 (s, CH$_3$)	123.34 (d, $J_{P,Rh}$ 278)
8 [Rh(PPh$_3$)$_2$Tp′]	7.5–6.9 {m, 30H, P(C$_6$H$_5$)$_3$}, 5.81 (s, 1H, pz H), 5.25 (s, 2H, pz H), 2.50 (s, 3H, CH$_3$), 2.28 (s, 6H, CH$_3$), 2.26 (s, 3H, CH$_3$), 1.79 (s, 6H, CH$_3$)[e]	149.92 (s, *C*CH$_3$), 147.49 (s, *C*CH$_3$), 146.47 (s, *C*CH$_3$), 142.66 (s, *C*CH$_3$), 135–127 {m, P(C$_6$H$_5$)$_3$}, 107.20 (s, pz CH), 105.94 (s, pz CH), 16.62 (s, C*C*H$_3$), 14.82 (s, C*C*H$_3$), 14.29 (s, C*C*H$_3$), 12.91 (s, pz C*C*H$_3$)[f]	41.64 (d, $J_{P,Rh}$ 175) 42.30 (dd, $J_{P,Rh}$ 179, $J_{P,P}$ 49), 39.18 (dd, $J_{P,Rh}$ 173, $J_{P,P}$ 51)[g]
	7.7–6.7 {m, 30H P(C$_6$H$_5$)$_3$}, 5.89 (s, 1H, pz H), 5.41 (brd s, 1H, pz H), 5.20 (br s, 1H, pz H), 2.63 (br s, 3H, CH$_3$), 2.35 (br s, 3H, CH$_3$), 2.31 s, 3H, CH$_3$), 2.25 (br s, 3H, CH$_3$), 2.12 (br s, 3H, CH$_3$), 1.43 (br s, 3H, CH$_3$)[g]		
11 [Rh(dppe)Tp′]	7.7–7.1 [m, 20H, {CH$_2$P(C$_6$*H*$_5$)$_2$}$_2$], 5.55 (s, 3H, pz CH), 2.20 (s, 9H, CH$_3$), 1.98 {dd, 4H, $^{2}J_{H,P}$ 12, $^{3}J_{H,P}$ 1, (C*H*$_2$PPh$_2$)$_2$}, 1.85 (s, 9H, CH$_3$)	148.86 (s, *C*CH$_3$), 145.34 (s, *C*CH$_3$), 136.40 [t, $J_{C,P}$ 19, {CH$_2$P(*C*$_6$H$_5$)$_2$}$_2$], 133.95 [t, $J_{C,P}$ 6, {CH$_2$P(*C*$_6$H$_5$)$_2$}$_2$], 129.28 [s, {CH$_2$P(*C*$_6$H$_5$)$_2$}$_2$], 127.86 [t, $J_{C,P}$ 5, {CH$_2$P(*C*$_6$H$_5$)$_2$}$_2$], 106.05 (s, pz CH), 30.57 {ddd, $^{1}J_{C,P}$ 49, $^{2}J_{C,P}$ 24, $^{2}J_{C,Rh}$ 2.5, (Ph$_2$P*C*H$_2$)$_2$}, 15.55 (s, CH$_3$), 13.53 (s, CH$_3$)	63.85 (d, $J_{P,Rh}$ 179)
12 [Rh(CO)(PPh$_3$)(HTp′)][BF$_4$]	11.84 (s, 1H, NH), 7.51–7.18 {m, 15H, P(C$_6$H$_5$)$_3$}, 6.01 (s, 1H, pz CH), 5.88 (s, 1H, pz CH), 5.65 (s, 1H, pz CH), 2.47 (s, 3H, CH$_3$), 2.42 (s, 3H, CH$_3$), 2.34 (s, 3H, CH$_3$), 1.84 (s, 3H, CH$_3$), 1.80 (s, 3H, CH$_3$), 1.46 (s, 3H, CH$_3$)	189.26 {dd, $J_{C,Rh}$ 70, $J_{C,P}$ 22, CO}, 153.47 (t, J 2, *C*CH$_3$), 152.51 (t, J 2, *C*CH$_3$), 151.61 (s, *C*CH$_3$), 148.67 (s, *C*CH$_3$), 147.90 (d, J 1, *C*CH$_3$), 145.77 (s, *C*CH$_3$), 145.55 (s, *C*CH$_3$), 134.2–128.8 {m, P(C$_6$H$_5$)$_3$}, 109.83 (s, pz CH), 107.61 (s, pz CH), 107.58 (s, pz CH), 15.64 (s, CH$_3$), 15.09 (d, J 2, CH$_3$), 13.18 (s, CH$_3$), 13.09 (s, CH$_3$), 11.45 (s, CH$_3$), 10.13 (s, CH$_3$)	41.38 (d, $J_{P,Rh}$ 158)

[a] Chemical shift (δ) in ppm, J values in Hz, spectra in CD_2Cl_2 at 20 °C unless stated otherwise. [b] See ref. 10. [c] At 0 °C. [d] At −60 °C. [e] At −20 °C. [f] At −40 °C. [g] At −80 °C.

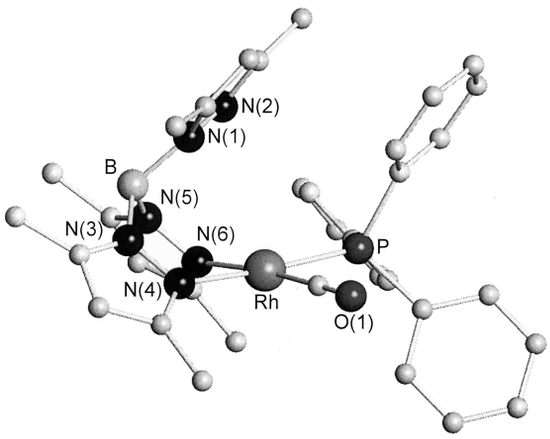

Fig. 1 The molecular structure of [Rh(CO)(PPh_3)Tp′] **2**. Hydrogen atoms in all structures shown except **12** have been omitted for clarity.

(HBR_3)] have been used[1,4,16] to distinguish between κ^2 and κ^3 co-ordination of hydrotris(pyrazolyl)borate ligands. Thus, a κ^3 isomer (form **C**, Scheme 1) shows ν(CO) at lower energy than does a κ^2 isomer (*ca.* 2060 and 1980 cm^{-1} *vs. ca.* 2080 and 2020 cm^{-1}); forms **A** and **B** cannot usually be distinguished in this way however. The ν(BH) stretching frequency of a co-ordinated hydrotris(pyrazolyl)borate ligand falls between *ca.* 2390 and 2590 cm^{-1} and, as a rule of thumb, κ^2 ν(BH) < 2480 cm^{-1} < κ^3 ν(BH). These ranges do not seem to be particularly affected by the geometry at the metal (octahedral, five-co-ordinate or square planar) but there is some overlap as ν(BH) is strongly influenced by the nature of the metal, the other ligands and the pyrazolyl ring substituents.[2,17] In the case of **1**, ν(CO) bands at 2058, 1982 cm^{-1} and ν(BH) at 2533 cm^{-1} in CH_2Cl_2, and at 2053, 1970 cm^{-1} and 2522 cm^{-1} in Nujol, correspond to κ^3 co-ordination both in solution and the solid state.

Carbonyl substitution by PR_3 ligands leads to structures which depend on the substituent R. For complexes **2**–**6**, **8**, **9**, and **11** the IR spectra reveal κ^2 co-ordination in both the solid state and in CH_2Cl_2 solution. The majority exist entirely in form **B** although [Rh(PPh_3)$_2$Tp] **9** shows two ν(BH) bands, at 2394s and 2414w cm^{-1} in Nujol, attributable to forms **A** and **B** respectively. The equilibrium is shifted in the direction of form **A** as a result of hydrogen atoms rather than methyl groups in the 5-positions of the pyrazolyl rings.[16]

Of the complexes [Rh(CO)LTp′], the $P(OPh)_3$ derivative **7** is unique in existing as an approximate 1 : 1 mixture of κ^2 and κ^3 isomers in CH_2Cl_2 solution {ν(CO) 2007 cm^{-1} (broad) and ν(BH) = 2520 and 2479 cm^{-1}} but in the solid state it is entirely κ^3 co-ordinated {ν(CO) 1984 cm^{-1} and ν(BH) 2519 cm^{-1}, form **C**}. This difference may be attributed to a decrease in both steric hindrance {the cone angle for $P(OPh)_3$ is 128° compared to 145° for PPh_3 and 170° for PCy_3} and electron density at the metal {$P(OPh)_3$ is a poorer donor and stronger π acceptor than the phosphine ligands}.[18]

The crystal structures of complexes 2–4 and 6–8

In order to confirm the solid state structures deduced from the IR spectra, single crystal X-ray diffraction studies were carried out on complexes **2**–**4** and **6**–**8**. The structures are shown in Figs. 1–6 and important bond lengths and angles are listed in Table 3. The rhodium atoms in **2**–**4**, **6** and **8** are κ^2 co-ordinated (*i.e.* as in form **B**) with the carbonyl and phosphine ligands completing square planar co-ordination of the rhodium as expected for the d^8 electron configuration of these rhodium(I) species. The bond lengths and angles around rhodium are of normal dimensions for such a ligand set.[19] The unco-ordinated pyrazolyl ring is orientated pseudo-parallel to the rhodium co-ordination plane. The Rh···B–N(1)–N(2) torsion angles (90, 103, 105, 102 and −75° respectively) reflect this orientation

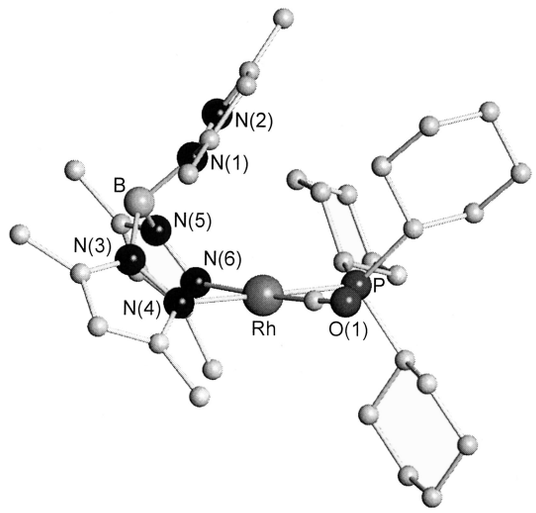

Fig. 2 The molecular structure of [Rh(CO)(PCy_3)Tp′] **3**.

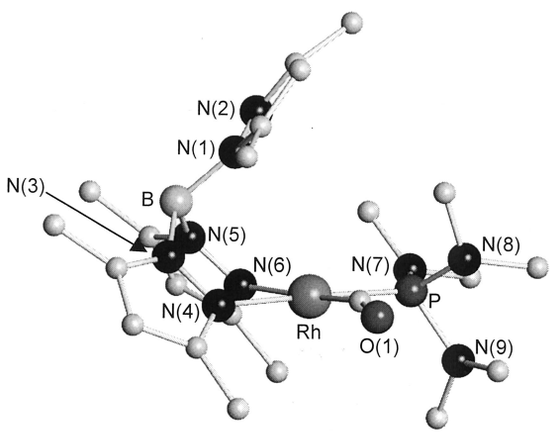

Fig. 3 The molecular structure of [Rh(CO){$P(NMe_2)_3$}Tp′] **4** showing one image of the disordered ligands.

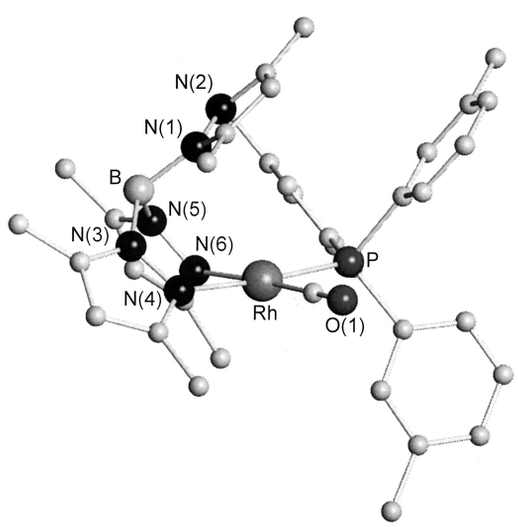

Fig. 4 The molecular structure of [Rh(CO){$P(C_6H_4Me$-*m*)$_3$}Tp′] **6**.

and result in Rh–N(2) separations of 3.537(5), 3.925(5), 3.854(5), 3.747(2) and 3.276(3) Å in **2**–**4**, **6** and **8** respectively. All of these distances are too long to be considered bonding and are essentially determined by the torsion about the B–N(1) bond. In **2**–**4** and **6** the unbound pyrazolyl ring is orientated so as to maximise the distance between the bulky phosphine ligand substituents and the 5-Me substituent. [Thus, N(2) is *syn* to the phosphorus atom in these cases.] In **8**, which has two phosphine ligands, N(2) is *syn* to P(2) and, presumably in order to

Table 3 Selected bond lengths (Å) and angles (°) for [Rh(CO)(PPh_3)Tp′] **2**, [Rh(CO)(PCy_3)Tp′] **3**, [Rh(CO){$P(NMe_2)_3$}Tp′] **4**, [Rh(CO){$P(C_6H_4Me\text{-}m)_3$}Tp′] **6**, [Rh(CO){$P(OPh)_3$}Tp′] **7**, [Rh(PPh_3)$_2$Tp′]·C_6H_{14} **8**·C_6H_{14}, [Rh(CO)(PPh_3)(HTp′)][BF_4]·thf **12**·thf, [Rh(CO)(PPh_3)Tp′][PF_6]·CH_2Cl_2 **2**$^+$[PF_6]$^-$·CH_2Cl_2 and [Rh(PPh_3)$_2$Tp′]X·3CH_2ClCH_2Cl **8**$^+$X$^-$·3CH_2ClCH_2Cl (X^- = [PF_6]$^-$ or [BF_4]$^-$)

	2	**3**	**4**	**6**	**7**	**8**	**12**	**2**$^+$[PF_6]$^-$	**8**$^+$[PF_6]$^-$	**8**$^+$[BF_4]$^-$
Rh–N(6)	2.1240(5)	2.142(4)	2.122(4)	2.098(2)	2.097(2)	2.081(2)	2.107(3)	2.093(3)	2.10(1)	2.110(6)
Rh–N(4)	2.108(4)	2.108(4)	2.112(5)	2.107(2)	2.109(2)	2.130(2)	2.092(3)	2.091(3)	2.18(1)	2.189(5)
Rh–N(2)	3.537(5)	3.925(5)	3.854(5)	3.747(2)	2.764(2)	3.276(3)	3.713(3)	2.224(4)	2.21(1)	2.236(5)
Rh–P	2.272(2)	2.292(1)	2.253(2)	2.280(1)	2.179(1)	2.256(1)[a]	2.265(1)	2.328(2)	2.338(3)[a]	2.351(2)[a]
Rh–C(1)	1.825(6)	1.798(5)	1.813(7)	1.81(1)	1.826(2)	—	1.823(4)	1.879(4)	—	—
Rh–P(2)	—	—	—	—	—	2.264(1)	—	—	2.349(3)	2.360(2)
N(6)–Rh–N(4)	83.7(2)	82.2(2)	83.1(2)	82.2(1)	81.9(1)	77.9(7)	84.0(1)	82.4(2)	80.5(3)	80.5(2)
N(4)–Rh–C(1)	92.4(2)	93.1(2)	90.3(3)	91.7(1)	95.0(1)	—	91.5(1)	94.7(2)	2.18(1)	2.189(5)
C(1)–Rh–P	86.0(2)	85.0(2)	85.5(2)	91.1(1)	86.9(1)	—	85.1(1)	90.0(2)	2.21(1)	2.236(5)
P–Rh–N(6)	98.3(1)	99.6(1)	101.3(1)	95.1(1)	96.2(1)	93.5(1)[a]	99.5(1)	92.4(2)	88.3(2)[a]	88.2(2)[a]
P(2)–Rh–N(6)	—	—	—	—	—	169.9(1)	—	—	160.7(3)	161.0(2)
N(2)–Rh–N(6)	—	—	—	—	90.8(1)	—	—	95.3(1)	95.5(3)	95.4(2)
N(2)–Rh–N(4)	—	—	—	—	77.7(1)	2.264(1)	—	84.2(1)	85.0(3)	85.2(2)
N(2)–Rh–C(1)	—	—	—	—	91.1(1)	—	—	93.7(2)	—	—
P(2)–Rh–P(1)	—	—	—	—	—	95.6(1)	—	—	98.7(1)	99.1(1)
N(2)–Rh–P	—	—	—	—	102.8(1)	—	—	98.6(1)	90.0(2)[a]	90.0(1)[a]
N(2)–Rh–P(2)	—	—	—	—	—	—	—	—	102.3(2)	102.0(2)
N(6)–Rh–C(1)	174.0(2)	173.8(2)	172.4(2)	173.6(1)	176.0(1)	—	175.4(1)	170.2(1)	—	—
N(4)–Rh–P	175.2(1)	177.8(1)	175.4(1)	175.0(1)	178.0(1)	169.1(1)[a]	176.0(1)	174.4(1)	167.2(2)[a]	167.2(2)[a]
N(4)–Rh–P(2)	—	—	—	—	—	93.5(1)	—	—	93.9(2)	93.5(2)
Rh···B–N(1)–N(2)	89.8(5)	103.4(4)	105.0(4)	101.7(2)	−19.1(2)	−75.2(2)	94.6(3)	−7.5(2)	−11.8(7)	−11.4(4)

[a] Parameter involving phosphorus atom labelled P(1).

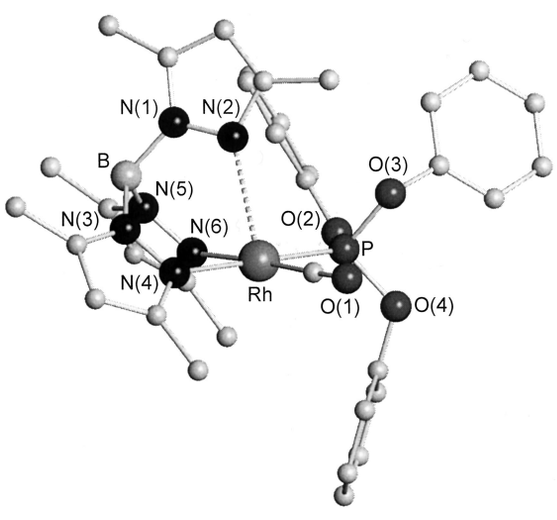

Fig. 5 The molecular structure of [Rh(CO){$P(OPh)_3$}Tp′] **7**.

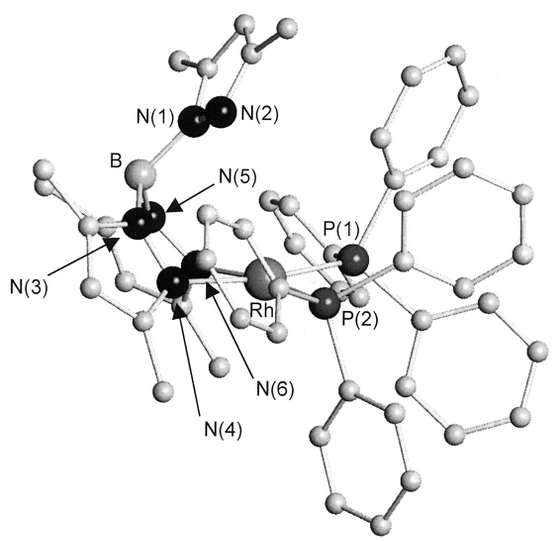

Fig. 6 The molecular structure of [Rh(PPh_3)$_2$Tp′]·C_6H_{14} **8**·C_6H_{14}.

minimise contacts between the 5-Me group and P(1) and its substituents, the Rh···B–N(1)–N(2) torsion angle has a lower magnitude (75°) than those of **2**–**4** and **6**.

As inferred from the IR spectrum, complex **7** adopts a different structure (Fig. 5). Although the rhodium to apical nitrogen distance [2.764(2) Å] is greater than the sum of the atomic radii of rhodium (1.345 Å) and nitrogen (0.71 Å) it is within the sum of the atomic radius of rhodium and the van der Waals radius of nitrogen (1.54 Å).[20] Moreover the Rh···B–N(1)–N(2) torsion angle is −19°, close to the ideal value for κ^3 co-ordination (*i.e. ca.* 0°, see below). The remaining co-ordination around Rh is close to that observed in the square planar species **2**–**4**, **6** and **8**. The co-ordination geometry in **7** is therefore distorted square pyramidal with the rhodium essentially in the plane of the basal ligands and with a very long Rh–apical ligand distance. This type of distorted co-ordination geometry for d^8 metals is well known in, for example, nickel(II) chemistry.[21] Similar co-ordination has been observed in other hydrotris(pyrazolyl)boratorhodium(I) species of the form [$Rh(CO)_2L'$] {L′ = hydrotris(5-methyl-3-trifluoromethylpyrazolyl)borate[16] and hydrotris(2*H*-benzo[*g*]-4,5-dihydroindazol-2-yl)borate[22]} and [RhL_2L'] {L_2 = *cis*-1,2-bis(diphenylphosphino)ethene, L′ = hydrotris(3,5-diisopropylpyrazolyl)borate}[15] for which Rh–N_{apical} distances are in the range 2.64 to 2.90 Å. Despite the spectroscopic indicators implying κ^3 co-ordination of the rhodium in these cases it is clear that the metal is much more strongly bound to two of the nitrogen atoms than to the third and that its geometry is closer to the κ^2 (**B**) form than true κ^3. However, the conformation of the Tp′ ligand in **8** is clearly close to that required for κ^3 co-ordination and presumably this is why its spectroscopic characteristics are close to those of conventional κ^3 HBR_3 complexes.

True κ^3 co-ordination in rhodium(I) complexes is known, for example in [Rh(η-C_2H_4)(CNR)Tp′] (R = 2,6-dimethylphenyl)[23] and [Rh{η-$C_2(CO_2Me)_2$}(PPh_3)Tp].[14] Remarkably, [Rh(η^4-nbd)Tp^{iPr}] [nbd = norbornadiene, Tp^{iPr} = hydrotris(3,5-diisopropylpyrazolyl)borate] crystallises with both κ^2 and κ^3 forms in the crystal.[2] The κ^2 isomer is of form **B**, is square planar at rhodium, and has Rh–N 2.134, 2.119 and 3.392 Å; the κ^3 form is trigonal bipyramidal (*TBPY*) at rhodium and has Rh–$N_{equatorial}$ 2.260 and 2.273 Å and Rh–N_{axial} 2.146 Å. This latter geometry is typical of κ^3 *TBPY* rhodium(I) complexes in having the axial Rh–N distance slightly less than the equatorial

Rh–N bond lengths. It is notable that in those cases where the κ^3 trigonal bipyramidal geometry is present the third equatorial site (*i.e.* that not occupied by the HBR_3 ligand) is occupied by a ligand that is a poor σ donor and good π acceptor (*e.g.* alkene or alkyne). The remaining axial site may be occupied by phosphine, alkene, isocyanide or other ligands.

The geometries and electronic structures of square pyramidal (*SPY*) and *TBPY* ML_5 species have been much studied. A helpful discussion of the literature by Albright *et al.*[24] noted that the axial M–L bond lengths in *TBPY* d^8 ML_5 species were typically ≤ equatorial bond lengths, in contrast to the situation in p-block chemistry. The preference of π-bonding ligands for equatorial sites in *TBPY* d^8 ML_5 complexes was also noted and explained by qualitative molecular orbital arguments. This preference arises because of the enhanced hybridisation and higher energy of the metal π-donor orbital in the equatorial plane compared with the essentially unhybridised dπ orbitals with which axial ligands interact. Finally, weakness of the $M–L_{apical}$ bond in *SPY* d^8 ML_5 complexes is also noted and explained in terms of the antibonding character of the d_{z^2}-apical ligand lone pair interaction especially in cases where the metal atom lies in the plane of the basal ligand (see also ref. 21). We have confirmed by EHMO calculations that the HOMO of species such as **7** is indeed the antibonding combination of the apical pyrazolyl nitrogen lone pair and the Rh d_{z^2} orbital. No quantitative prediction is easily made as to the relative likelihood of κ^3-*SPY* and κ^3-*TBPY* geometries for a given $[Rh^IL_2(HBR_3)]$ complex although the observation that both forms are present in the same crystal of $[Rh(\eta^4\text{-nbd})Tp^{iPr}]$[2] implies that the balance may be very delicately poised. In cases such as **7** it seems likely that the conformation of the $P(OPh)_3$ ligand in the crystal is not compatible with the usual pyrazolyl conformation in κ^2-HBR_3 ligands (see Fig. 5) because of unfavourable Ph–pyrazolyl contacts. The spectroscopic observation of a κ^2 isomer of **7** in solution implies that other conformers are available to the $P(OPh)_3$ and Tp′ ligands.

NMR spectroscopy and the fluxional behaviour of [Rh(CO)LTp′] and [RhL_2Tp']

The structural variations in [Rh(CO)LTp′] and [RhL_2Tp'], described above, are mirrored in their NMR spectra, most of the complexes showing fluxional behaviour involving interconversion between the various possible isomers. For some complexes, however, overlap of the peaks of the ligands L with those of the Tp′ ligand prevented studies of the fluxional process in detail.

At 20 °C, all three pyrazolyl rings of complexes **2**, **4**–**7** and **11** are equivalent due to fast exchange of co-ordinated and unco-ordinated pyrazolyl rings on the NMR timescale, *i.e.* equilibration between forms **B** and **C**. At low temperature, the ^{1}H NMR spectrum of **2** is broadened but still not resolved at −80 °C. However, the more sterically hindered species, **3** and **8**–**10**, have extremely broad spectra even at room temperature due to the slower exchange of co-ordinated and unco-ordinated pyrazolyl rings.

Of the carbonylphosphine complexes, [Rh(CO)(PCy_3)Tp′] **3** has the most sterically hindered and most electron rich metal centre. At room temperature, two broad pyrazolyl hydrogen peaks (integration 2:1) are observed but at 0 °C they become sharp as the fluxional process which renders all three pyrazolyl rings equivalent is quenched on the NMR timescale. At −40 °C the higher field peak begins to split further and, at −60 °C, all three pyrazolyl rings are inequivalent; there are three sharp pyrazolyl hydrogen peaks and five sharp methyl hydrogen peaks (the sixth is obscured by PCy_3 resonances) (Table 2). Thus, between 0 and −60 °C a second fluxional process (which gives rise to a 2:1 ratio of pyrazolyl rings) is slowed on the NMR timescale. At room temperature the ^{13}C-{^{1}H} NMR spectrum of **3** is very broad and only the doublet of doublets for CO (coupling to ^{31}P and ^{103}Rh) is well resolved. However, at −60 °C, all three pyrazolyl rings are inequivalent (Table 2).

The room temperature ^{1}H NMR spectrum of the bis(phosphine) complex [Rh(PPh_3)$_2$Tp′] **8** shows a very broad pyrazolyl hydrogen signal and one sharp and one broad methyl peak. At −20 °C this is resolved into two pyrazolyl hydrogen peaks and four methyl peaks; at lower temperature the signal broadens further and at −80 °C there are six broad methyl peaks. Thus, at −80 °C all three pyrazolyl rings are starting to become inequivalent, as found for **3**. At room temperature the ^{31}P NMR spectrum of **8** shows equivalent phosphorus atoms giving rise to a sharp doublet at δ 41.6 ($J_{P,Rh}$ = 175 Hz). However, at −80 °C this signal is resolved into two doublets of doublets, at δ 42.3 ($J_{P,Rh}$ = 179, $J_{P,P}$ = 49 Hz) and 39.2 ($J_{P,Rh}$ = 173, $J_{P,P}$ = 51 Hz); the phosphorus atoms become inequivalent, on the NMR timescale, presumably because of the fixed orientation of the unbound pyrazolyl ring. {If so, this would be the first rhodium hydrotris(pyrazolyl)borate complex in which the rotational motion of the free pyrazolyl ring is frozen on the NMR timescale.}

The room temperature ^{1}H NMR spectrum of [Rh(PPh_3)$_2$Tp] **9** in CD_2Cl_2 or $CDCl_3$ is again very broad and only shows strong signals for the phenyl ring protons in PPh_3 (between δ 7.6 and 7.0). There are also two very broad peaks at *ca.* δ 5.8 and 6.4. (This spectrum differs from that previously assigned.)[14] As the temperature is lowered, the broad resonances begin to sharpen and split, until at −40 °C there are several new peaks between δ 8.21 and 5.54; others may be obscured by the phenyl resonances. Many of these peaks are still broad at −40 °C and at lower temperatures several begin to broaden further. No assignment of these spectra has been possible.

The room temperature ^{31}P NMR spectrum of [Rh(PPh_3)$_2$Tp] **9** in CD_2Cl_2 shows a broad doublet at δ 50.9 ($J_{P,Rh}$ = 165 Hz), in this case in agreement with the reported data.[14] At −40 °C this signal splits into two doublets of approximately equal intensity, at δ 51.0 ($J_{P,Rh}$ = 174) and 49.3 ($J_{P,Rh}$ = 176 Hz). However, at −80 °C the latter is broadened due to partial resolution of another fluxional process. Unlike the Tp′ analogue, **8**, the two signals at −40 °C cannot be attributed to a single isomer with inequivalent phosphorus atoms because two doublets of doublets would be expected. Moreover, broadening of the doublet at δ 49.3 shows fluxionality which is independent of the doublet at δ 51.0. As noted above, the IR spectrum of **9** suggested two different κ^2 co-ordinated species in the solid state; *i.e.* forms **A** and **B**. The ^{31}P NMR signal at δ 51.0 is assigned to form **A** which is symmetrical and can only give a doublet even at lower temperatures. That at δ 49.3 is assigned to form **B** which can give a doublet of doublets. The proposal of form **A** for the Tp complex **9**, but not for the Tp′ analogue **8**, is consistent with the observation that substituents in the 5 position of the pyrazolyl ring shift the equilibrium from form **A** in the direction of form **B**.[16]

The X-ray structural studies on complexes **2**–**4** and **6**, described above, provide some insight into the dynamic NMR spectroscopic properties, particularly of **3** which showed the best resolved NMR spectra. Scheme 2 indicates a series of possible equilibria between various *SPY* and *TBPY* forms of a [Rh(CO)(PR_3)Tp′] complex such as **2**–**4** or **6**. The X-ray structural and spectroscopic data imply that a structure such as *SPY*(2) in Scheme 2, in which there is a weak apical contact between Rh and N(2) (as seen in the crystal structure of **7**), is easily accessible from the κ^2 square planar structure *SP*(2). The existence of stable κ^3-*TBPY* isomers of [RhL(PR'_3)-(HBR_3)] species noted above implies that of the various isomeric *TBPY* intermediates (or transition states, we will assume the former for the purposes of the discussion below) that might be invoked, that with the phosphine axial and the better π-acceptor ligand (here CO) equatorial would be the most stable, as shown in Scheme 2 [*TBPY*(P_{ax})]. If this isomer is thermally accessible then once formed it affords access to an

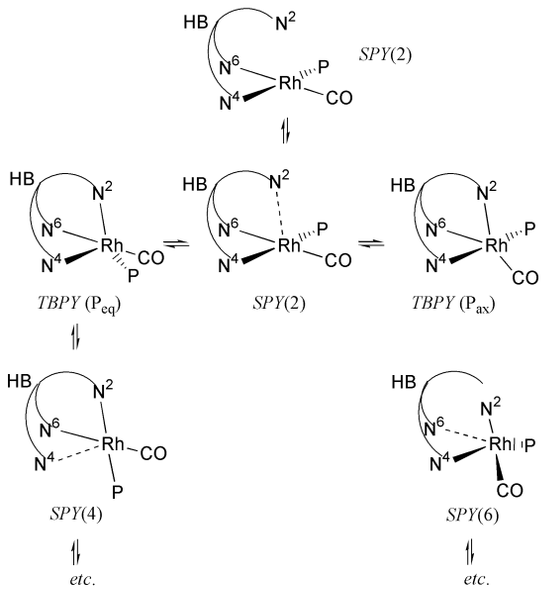

Scheme 2

SPY [Rh(CO)(PR_3)Tp′] in which N(6) now occupies the apical site and hence N(2) and N(6) have been permuted [see *SPY*(6) in Scheme 2]. If the interconversion of *SPY*(2), *TBPY*(P_{ax}) and *SPY*(6) is rapid on the NMR timescale the pyrazolyl rings at N(2) and N(6) become equivalent. In order for all three pyrazolyl rings to become equivalent it is necessary to obtain access to species in which N(4) occupies the apical site [*SPY*(4) in Scheme 2]. These are only available through a second *TBPY* intermediate [*TBPY*(P_{eq}) in Scheme 2] which is isomeric with the first, and likely to be of higher energy having the better π-acceptor ligand, CO, in the axial site and the phosphine in the equatorial plane. Further permutation of the environments of the N(2), N(4) and N(6) sites by analogous processes leads to equivalence of all three pyrazolyl rings. This mechanism (which is of course related to Berry pseudo-rotation and its turnstile variant) is consistent with the observed higher energy of activation for the process leading to equivalence.

Voltammetric studies

Cyclic voltammetric studies show that all of the rhodium(I) complexes **2**–**11** undergo electron-transfer reactions and, as described below, chemical oxidation gives the corresponding, isolable, rhodium(II) complexes. However, the cyclic voltammetry is affected by the structural changes which accompany oxidation (see below) and $E^{\circ\prime}$ cannot be calculated simply from the average of the peak potentials, $(E_p)_{ox}$ and $(E_p)_{red}$. (Estimated oxidation potentials, quoted *vs.* the $[Fe(\eta\text{-}C_5H_5)_2]^+$–$[Fe(\eta\text{-}C_5H_5)_2]$ couple at 0.0 V, are given in Table 1.) A more detailed analysis of these voltammetric data and discussions of the mechanism of the oxidative isomerisation process and of the effects on electrochemical behaviour of added mediators such as $[Fe(\eta\text{-}C_5H_5)_2]$ and $[Pd(mnt)_2]^-$ {mnt = $[S_2C_2(CN)_2]^{2-}$} will be published elsewhere.[25] Here we give an overview sufficient to relate the observed electrochemistry qualitatively to (i) the oxidatively induced structural changes, and (ii) the dependence of the fluxionality of [Rh(CO)LTp′] on the ligand L.

At a glassy carbon electrode in CH_2Cl_2, $[Rh(CO)_2Tp']$ **1** undergoes one-electron oxidation ($E^{\circ\prime} = 0.15$ V) which is only fully reversible at scan rates greater than 200 mV s^{-1}; in thf, the oxidation process is irreversible.

As described above, complex **7** exists as an approximate 1 : 1 mixture of the κ^2 and κ^3 isomers in CH_2Cl_2 solution. It is reversibly oxidised at glassy carbon ($E^{\circ\prime} = -0.17$ V) and platinum electrodes ($E^{\circ\prime} = -0.15$ V) with peak-to-peak separations comparable to those for the oxidation of $[Fe(\eta\text{-}C_5Me_5)_2]$ at scan rates of 20 mV s^{-1} to 2 V s^{-1}. Complexes **2**, **4**–**6** and **11** are κ^2 co-ordinated in CH_2Cl_2 but at room temperature the co-ordinated and unco-ordinated pyrazolyl rings are rendered equivalent by exchange which is rapid on the NMR timescale. They are reversibly oxidised at a glassy carbon electrode but at a platinum electrode the waves are often irreproducible, with broadened oxidation peaks and far greater peak-to-peak separations than those of the calibrant, $[Fe(\eta\text{-}C_5H_5)_2]$ or $[Fe(\eta\text{-}C_5Me_5)_2]$.

Complexes [Rh(CO)(PCy_3)Tp′] **3** and $[Rh(PPh_3)_2L']$ {L′ = Tp′ **8**, Tp **9** or $B(pz)_4$ **10**} are also κ^2 co-ordinated in solution but NMR spectroscopy showed that exchange of co-ordinated and unco-ordinated pyrazolyl rings is slower than for the other carbonyl phosphine complexes. In agreement, the cyclic voltammograms of **3** and **8**–**10** in CH_2Cl_2 show broad one-electron oxidation waves with very large peak-to-peak separations even at a glassy carbon electrode, consistent with slow electron transfer due to structural changes accompanying oxidation.

Synthesis and characterisation of rhodium(II) complexes

On the basis of the potentials given in Table 1, the rhodium(I) species **2**–**11** have been chemically oxidised with the ferrocenium ion. The resulting cations, $\mathbf{2}^+$–$\mathbf{11}^+$, are rare examples of well characterised mononuclear rhodium(II) complexes;[26] others are $[Rh(C_6Cl_5)_4]^{2-}$,[27] $[RhH(CO)(PPh_3)_3]^+$,[28] $[Rh(bpca)_2]$ {bpca = bis(2-pyridylcarbonyl)amide}, and $[Rh(bpca)(tpy)]^+$ (tpy = 2,2′ : 6′2″-terpyridyl).[29] Interestingly, in light of the oft cited analogy between Tp′ and $\eta\text{-}C_5R_5$ ligands,[3,30] the cyclopentadienyl complexes are considerably less stable than their hydrotris(pyrazolyl)borate analogues; $[Rh(CO)(PPh_3)(\eta\text{-}C_5H_5)]^+$ dimerises on oxidation, giving the fulvalene dication $[Rh_2(CO)_2(PPh_3)_2(\eta^5\text{:}\eta'^5\text{-}C_{10}H_8)]^{2+}$.[31] (The observation that $[Rh(CO)(PPh_3)(\eta\text{-}C_5H_5)]$ {$(E_p)_{ox} = 0.0$ V} appears to be oxidised at a more positive potential than [Rh(CO)(PPh$_3$)Tp′] (−0.16 V, in thf) seems to support the generally held view that Tp′ is a better donor ligand than $\eta\text{-}C_5H_5$. However, it is now clear[32] that no such generality is valid.)

Although the potential for the oxidation is thermodynamically unfavourable, complex **1** reacts with $[Fe(\eta\text{-}C_5H_5)_2][PF_6]$ ($E^{\circ\prime} = 0.0$ V) in CH_2Cl_2 solution to give, as the final product, a yellow solution of the *N*-protonated rhodium(I) complex $[Rh(CO)_2(HTp')][PF_6]$[6,33] (HTp′ = ligand in which one of the three pyrazolyl rings of Tp′ is *N*-protonated) (see below); ESR spectroscopy (see below) indicates initial one-electron transfer gives $[Rh(CO)_2Tp']^+$ $\mathbf{1}^+$.

The rhodium(II) cation $\mathbf{1}^+$ is also implicated in the oxidative substitution of **1**. Thus, the CV of a 1 : 1 mixture of **1** and PPh_3 in thf shows an irreversible oxidation wave accompanied by a product wave at a potential consistent with the formation of $[Rh(CO)(PPh_3)Tp']^+$ $\mathbf{2}^+$ (see below) by a rapid reaction between $[Rh(CO)_2Tp']^+$ and PPh_3. Moreover, addition of $[Fe(\eta\text{-}C_5H_5)_2][PF_6]$ to a mixture of **1** and PPh_3 in CH_2Cl_2 gave a green solution of $\mathbf{2}^+$; oxidative substitution was complete after two minutes (*cf.* the reaction between **1** and PPh_3 in *n*-hexane, which requires heating under reflux for 24 hours) providing a direct and rapid route to $\mathbf{2}^+$ from **1**.

Addition of $[Fe(\eta\text{-}C_5H_5)_2][PF_6]$ to CH_2Cl_2 solutions of complexes **2**, **4**–**6**, **8** and **11** at 0 °C gave green or purple solutions of the cations $[Rh(CO)LTp']^+$ {L = PPh_3 $\mathbf{2}^+$, $P(NMe_2)_3$ $\mathbf{4}^+$, $P(C_6H_4Me\text{-}p)_3$ $\mathbf{5}^+$ or $P(C_6H_4Me\text{-}m)_3$ $\mathbf{6}^+$}, $[Rh(PPh_3)_2Tp']^+$ $\mathbf{8}^+$ or [Rh(dppe)Tp′]$^+$ $\mathbf{11}^+$, isolated as their $[PF_6]^-$ salts. The tetrafluoroborate salt $\mathbf{8}^+[BF_4]^-$ was prepared similarly. Complexes $\mathbf{2}^+[PF_6]^-$, $\mathbf{4}^+[PF_6]^-$ and $\mathbf{8}^+[PF_6]^-$ are stable in the solid state and moderately stable in solution whereas $\mathbf{5}^+[PF_6]^-$ and $\mathbf{6}^+[PF_6]^-$ are much more prone to decomposition, forming *N*-protonated rhodium(I) complexes related to $[Rh(CO)_2(HTp')][PF_6]$; the salt $\mathbf{11}^+[PF_6]^-$ decomposed in air to give an

Table 4 ESR spectroscopic data for rhodium(II) complexes[a]

Complex	g_1	g_2	g_3	g_{ave}	g_{iso}	$A_1(^{103}Rh)$	$A_2(^{103}Rh)$	$A_3(^{103}Rh)$	$A_1(^{14}N)$	$A_2(^{14}N)$	$A_3(^{14}N)$	$A_3(^{31}P)$
$\mathbf{1}^+$	2.318	2.147	1.989	2.151	—	22	—	24.5(5)	26	27.2(2)	31.3(3)	—
$\mathbf{2}^+$	2.256	2.163	1.993	2.137	2.143	17	—	28.9(2)	25	25.8(5)	27.7(4)	4.8(5)
$\mathbf{3}^+$	2.277	2.167	1.993	2.146	2.155	—	—	25.8(3)	—	—	28.8(6)	4.9
$\mathbf{4}^+$	2.234	2.157	1.995	1.129	2.132	21.1(9)	10.1(3)	28.3(2)	21.1(9)	24.4(2)	28.3(2)	—
$\mathbf{5}^+$	2.260	2.164	1.993	2.139	2.144	21	—	25.6(1)	21	25	29.3(1)	7.1(1)
$\mathbf{6}^+$	2.256	2.161	1.994	2.137	2.144	18	10.4(3)	25.6(1)	25	24.9(2)	29.4(1)	6.2(2)
$\mathbf{7}^+$	2.233	2.220	1.993	2.142	2.154	—	—	27.1(3)	—	—	27.8(1)	—
$\mathbf{8}^+$	2.282	2.250	1.994	2.175	2.196	—	—	21.1(2)	—	—	24.3(5)	6.3(7)
$\mathbf{9}^+$	2.262	2.224	1.994	2.160	2.183	—	—	23.4(1)	—	—	27.2(1)	—
$\mathbf{10}^+$	2.264	2.231	1.995	2.163	2.181	—	—	23.9(1)	—	—	26.7(1)	—
$\mathbf{11}^+$	2.287	2.231	1.991	2.170	2.187	—	—	26.0(2)	—	—	24.7(1)	10.8(1)

[a] Anisotropic spectra were computer-simulated; *A* values for less well resolved features were analysed by least-squares fits of portions of the spectra by sets of Gaussian absorption lines. Hyperfine couplings in 10^{-4} cm^{-1}.

unidentified bright yellow solid the ν(BH) stretch of which was inconsistent with the formation of an *N*-protonated complex.

Addition of $[Fe(\eta\text{-}C_5H_5)_2][PF_6]$ to [Rh(CO)(PCy_3)Tp′] **3** or [Rh(CO){$P(OPh)_3$}Tp′] **7** in CH_2Cl_2 gave green solutions of the extremely reactive cations $\mathbf{3}^+$ or $\mathbf{7}^+$ which form the *N*-protonated complexes $[Rh(CO)L(HTp')]^+$ {L = PCy_3 or $P(OPh)_3$} in less than five minutes. At −78 °C the rhodium(II) cations were more stable, but still decomposed slowly. Addition of $[Fe(\eta\text{-}C_5H_5)_2][PF_6]$ to CH_2Cl_2 solutions of **9** or **10** at 0 °C gave purple solutions of $[Rh(PPh_3)_2L']^+$ {L′ = Tp $\mathbf{9}^+$ or $B(pz)_4$ $\mathbf{10}^+$}. Addition of diethyl ether followed by *n*-hexane gave purple solids $\mathbf{9}^+[PF_6]^-$ and $\mathbf{10}^+[PF_6]^-$ which decomposed very rapidly on exposure to air.

Complexes $\mathbf{2}^+$, $\mathbf{4}^+$–$\mathbf{6}^+$, $\mathbf{8}^+$ and $\mathbf{11}^+$, as their $[PF_6]^-$ salts, were characterised by elemental analysis, IR, UV-visible (Table 1) and ESR spectroscopy (Table 4) and by cyclic voltammetry which showed reduction waves corresponding to reformation of the neutral rhodium(I) analogues. Complex $\mathbf{10}^+$ decomposed before characterisation was possible, but $\mathbf{9}^+$ was characterised by elemental analysis and ESR spectroscopy. (The especially high reactivity of these complexes relative to $\mathbf{8}^+$ may stem from the reduced steric hindrance around the metal. The cone angle of Tp′ is 236°, which reflects the enclosure of the metal in a protective pocket of methyl substituents, but that of Tp is only 199°.[3]) In addition, $[Rh(CO)(PPh_3)Tp'][PF_6]\cdot CH_2Cl_2$ $\mathbf{2}^+[PF_6]^-\cdot CH_2Cl_2$, $[Rh(CO)\{P(NMe_2)_3\}Tp'][PF_6]\cdot CH_2ClCH_2Cl\cdot 0.5H_2O$ $\mathbf{4}^+[PF_6]^-\cdot CH_2ClCH_2Cl\cdot 0.5H_2O$ (incompletely, see below) and $[Rh(PPh_3)_2Tp']X\cdot 3CH_2ClCH_2Cl$ (X = PF_6 or BF_4) $\mathbf{8}^+X^-\cdot 3CH_2ClCH_2Cl$ have been structurally characterised by X-ray crystallography.

The CO and BH stretching frequencies for the rhodium(II) complexes are given in Table 1. Solutions of the cations were prepared under a nitrogen atmosphere and Nujol mulls were prepared in air. IR spectra of the cations $\mathbf{2}^+$, $\mathbf{4}^+$ and $\mathbf{8}^+$ were obtained without decomposition whereas considerable decay occurred during preparation of the Nujol mulls of $\mathbf{5}^+$, $\mathbf{6}^+$ and $\mathbf{11}^+$. Attempts to prepare a Nujol mull of $\mathbf{9}^+$ under argon were unsuccessful, and complexes $\mathbf{3}^+$ and $\mathbf{7}^+$ were detected only in solution.

For each rhodium(II) cation ν(CO) is approximately 90 cm^{-1} higher than that of the analogous neutral complex. The ν(BH) values occur between 2556 and 2558 cm^{-1}, approximately 85 cm^{-1} higher in energy than for the rhodium(I) analogues. When an increase in the positive charge of a complex is not accompanied by a change in the bonding mode of the hydrotris(pyrazolyl)borate ligand ν(BH) rises by *ca.* 10–20 cm^{-1}, irrespective of whether the metal centre changes oxidation state. For example, a 13–14 cm^{-1} increase is observed for the κ^3 co-ordinated redox pairs $[WCl(CO)(\eta^2\text{-}MeC{\equiv}CMe)Tp']^z$ {ν(BH)(CH_2Cl_2) 2555 ($z = 0$) and 2569 cm^{-1} ($z = 1$)} and $[WBr(CO)(\eta^2\text{-}MeC{\equiv}CMe)Tp']^z$ {ν(BH)(CH_2Cl_2) 2556 ($z = 0$) and 2569 cm^{-1} ($z = 1$) respectively} in which tungsten has formal oxidation states II and III.[34] Similarly, an increase of 11–18 cm^{-1} in ν(BH) is found for the redox pairs $[RhL(o\text{-}O_2C_6Cl_4)Tp']^z$ {$z = 0$ or 1; L = PPh_3, $AsPh_3$, $P(OPh)_3$ or py} in which rhodium remains in oxidation state III, and the *o*-catecholate ligand, $o\text{-}O_2C_6Cl_4^{2-}$, is oxidised to a semiquinone.[35] The difference in ν(BH) for κ^2 and κ^3 isomers is considerably larger. For example, in CH_2Cl_2 each of the complexes [Rh(CO){$P(OPh)_3$}Tp′] **7** and [Rh(η^4-nbd)L′] {nbd = norbornadiene, L′ = hydrotris(3,5-diisopropylpyrazolyl)borate}[2] exists in an approximate 1:1 ratio of the κ^2 and κ^3 co-ordinated forms [ν(BH) 2479, 2520 and 2481, 2545 cm^{-1} respectively], the difference in ν(BH) for the two forms being 41 and 64 cm^{-1} respectively.

These data suggest, therefore, that on oxidation of $[RhL_2Tp']$ only 10–20 cm^{-1} of the increase in ν(BH) results from the positive charge on the cation, with the additional 60–70 cm^{-1} increase resulting from κ^2 to κ^3 isomerisation.

All of the carbonyl phosphine cations $[Rh(CO)LTp'][PF_6]$ are green, except for $[Rh(CO)\{P(NMe_2)_3\}Tp'][PF_6]$ $\mathbf{4}^+$ which is purple, and all of the bis(phosphine) or ditertiary phosphine complexes are purple, except for [Rh(dppe)Tp′][PF_6] $\mathbf{11}^+$ which is olive green. The UV-visible spectra of $[Rh(CO)LTp'][PF_6]$ {L = PPh_3 $\mathbf{2}^+$, $P(NMe_2)_3$ $\mathbf{4}^+$, $P(C_6H_4Me\text{-}p)_3$ $\mathbf{5}^+$ or $P(C_6H_4Me\text{-}m)_3$ $\mathbf{6}^+$} and $[Rh(PPh_3)_2Tp'][BF_4]$ $\mathbf{8}^+$ in CH_2Cl_2 are given in Table 1 with approximate values of the absorption coefficient ε for $\mathbf{2}^+$, $\mathbf{4}^+$ and $\mathbf{8}^+$. (Complexes $\mathbf{5}^+$ and $\mathbf{6}^+$ partially decomposed while the spectra were being recorded so that no quantitative measurements were possible, and the spectra of $\mathbf{9}^+$ and $\mathbf{11}^+$ were not obtained due to their air sensitivity.)

The crystal structures of the rhodium(II) complexes $\mathbf{2}^+$, $\mathbf{4}^+$ and $\mathbf{8}^+$

The structures of the three rhodium(II) cations, $\mathbf{2}^+$, $\mathbf{4}^+$ (incomplete, see below) and $\mathbf{8}^+$, including two salts of the last, have been determined by X-ray crystallography. There is good agreement between the structural data for $\mathbf{8}^+[PF_6]^-$ and $\mathbf{8}^+[BF_4]^-$ (Table 3) which indicates that the geometry of the cation is not significantly influenced by crystal packing forces. The latter structure is considerably more precise and is used in the discussion below.

The structure of the cation $\mathbf{2}^+$ is shown in Fig. 7 and that of the cation of the $[BF_4]^-$ salt of $\mathbf{8}^+$ in Fig. 8; important bond lengths and angles are collected in Table 3. The incomplete analysis of $\mathbf{4}^+$ indicates that it has the expected connectivity and general structure. There is a marked change in co-ordination about rhodium on one-electron oxidation, from square planar in the neutral κ^2 rhodium(I) complexes to square pyramidal in the κ^3 rhodium(II) cations. The apical Rh–N(2) bond in $\mathbf{2}^+$ [2.22(1) Å] is longer than those in the basal plane [approximately 2.09(1)], but considerably shorter than $Rh\text{–}N_{apical}$ in the neutral square pyramidal complex [Rh(CO){$P(OPh)_3$}Tp′] **7** [2.764(2) Å]. In addition, the Rh ··· B–N(1)–N(2) torsion angle decreases on oxidation, from *ca.* 90° to near zero (−8° in $\mathbf{2}^+$),

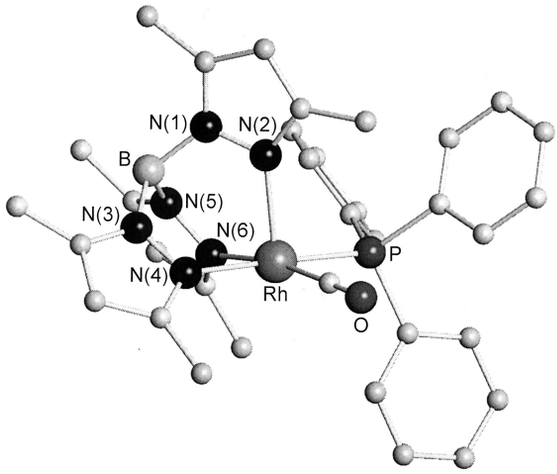

Fig. 7 The molecular structure of the cation $[Rh(CO)(PPh_3)Tp']^+$ in $[Rh(CO)(PPh_3)Tp'][PF_6]\cdot CH_2Cl_2$ $\mathbf{2}^+[PF_6]^-\cdot CH_2Cl_2$.

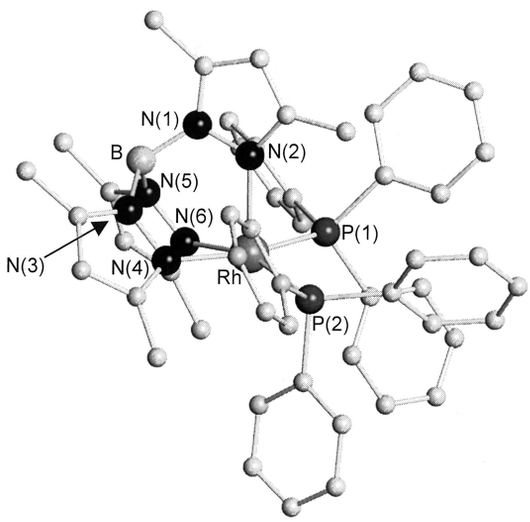

Fig. 8 The molecular structure of the cation $[Rh(PPh_3)_2Tp']^+$ in $[Rh(PPh_3)_2Tp'][BF_4]\cdot 3CH_2ClCH_2Cl\cdot\mathbf{8}^+[BF_4]^-\cdot 3CH_2ClCH_2Cl$.

the required orientation for co-ordination of N(2) to rhodium and formation of the κ^3 geometry.

Cation $\mathbf{8}^+$ is also square pyramidal but with a greater distortion from the ideal geometry than $\mathbf{2}^+$. The Rh–N(2) bond length for $\mathbf{8}^+$ is 2.236(5) Å (similar to that of $\mathbf{2}^+$) and the Rh···B–N(1)–N(2) torsion angle is −11° compared to 75° for neutral **8**. The equatorial Rh–N(4) distance is longer than Rh–N(6) [2.189(5) Å compared to 2.110(6) Å in $\mathbf{8}^+$], and P(2), which is *trans* to the shorter Rh–N(6) bond, is pushed away from the axial pyrazolyl ring [N(2)–Rh–P(2) 102.0(2)° and N(6)–Rh–P(2) 161.0(2)°, *cf.* N(2)–Rh–P(1) 90.0(1)° and N(4)–Rh–P(1) 167.2(2)°]. The reduction of the Rh···N(2) distance from *ca.* 2.6 or 2.7 Å in species with structures such as that of **7** to *ca.* 2.25 Å in $\mathbf{2}^+$ or $\mathbf{8}^+$ and the ESR spectra (see below) are fully consistent with the apical interaction in these d^7 rhodium(II) complexes being of the form shown in Fig. 9. Thus the SOMO is of Rh···N(2) σ* character.

ESR spectroscopy of rhodium(II) complexes

In order to probe the electronic structure of the rhodium(II) complexes, ESR spectra were recorded in both fluid and frozen solution. The spectra of analytically pure samples of the complexes $\mathbf{2}^+$, $\mathbf{4}^+$, $\mathbf{8}^+$ and $\mathbf{9}^+$ (as their $[PF_6]^-$ salts) were recorded in 1:1 CH_2Cl_2–1,2-dichloroethane. The less stable species were generated *in situ* by treating the neutral complex with $[Fe(\eta\text{-}C_5H_5)_2][PF_6]$ or $[Fe(\eta\text{-}C_5H_5)(\eta\text{-}C_5H_4COMe)][PF_6]$.

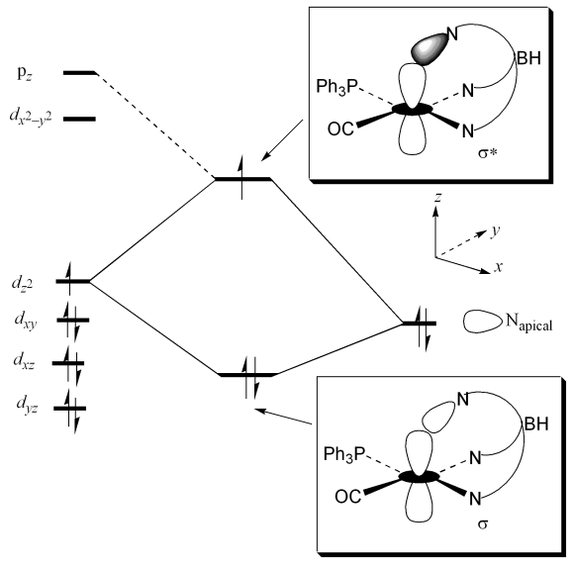

Fig. 9 Schematic orbital interaction diagram for the apical Rh···N bond in complex $\mathbf{2}^+$.

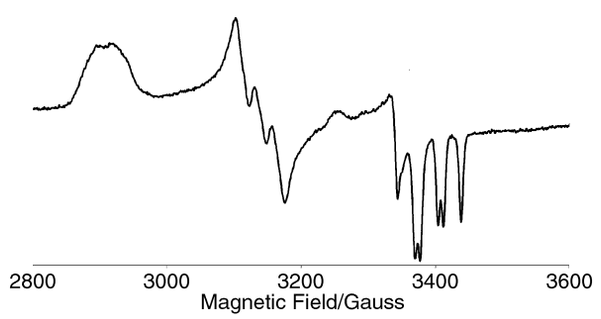

Fig. 10 The anisotropic ESR spectrum of $[Rh(CO)_2Tp']^+$ $\mathbf{1}^+$ at 100 K in CH_2Cl_2–1,2-dichloroethane (1:1).

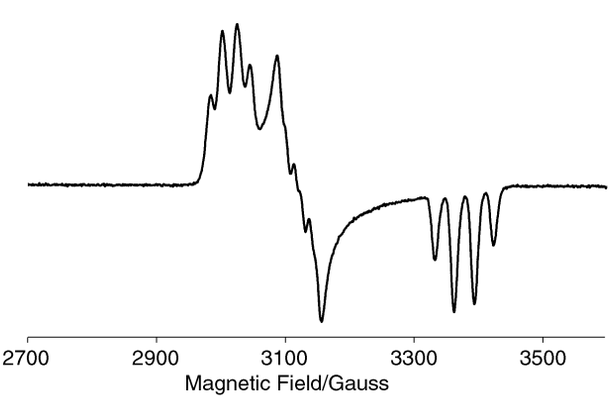

Fig. 11 The anisotropic ESR spectrum of $[Rh(CO)\{P(NMe_2)_3\}Tp']^+$ $\mathbf{4}^+$ at 120 K in CH_2Cl_2–1,2-dichloroethane (1:1).

The anisotropic ESR spectra of $[Rh(CO)_2Tp']^+$ $\mathbf{1}^+$, $[Rh(CO)\{P(NMe_2)_3\}Tp']^+$ $\mathbf{4}^+$, $[Rh(CO)\{P(C_6H_4Me\text{-}m)_3\}Tp']^+$ $\mathbf{6}^+$, and $[Rh(PPh_3)_2Tp']^+$ $\mathbf{8}^+$ are shown in Figs. 10–13 and g and A values are collected in Table 4. The isotropic spectrum of $[Rh(CO)\{P(NMe_2)_3\}Tp']^+$ $\mathbf{4}^+$ shows four partially resolved hyperfine lines due to coupling to one $I = 1$ and one $I = 1/2$ nucleus [$A_N = 25.1(1)$ and $A_{Rh} = 17.4(1)$]. All other isotropic spectra consist of a broad line at g_{iso} *ca.* 2.13–2.19.

In the frozen-solution spectra of $[Rh(CO)\{P(OPh)_3\}Tp']^+$ $\mathbf{7}^+$ and all four bis(phosphine) or ditertiary phosphine cations ($\mathbf{8}^+$–$\mathbf{11}^+$) no hyperfine structure was resolved for the central and low-field features. All other frozen-solution spectra showed resolved structure for all three components of the g matrix.

The high-field features were generally best resolved, with coupling to one $I = 1$ nucleus (^{14}N) and two $I = 1/2$ nuclei (^{103}Rh

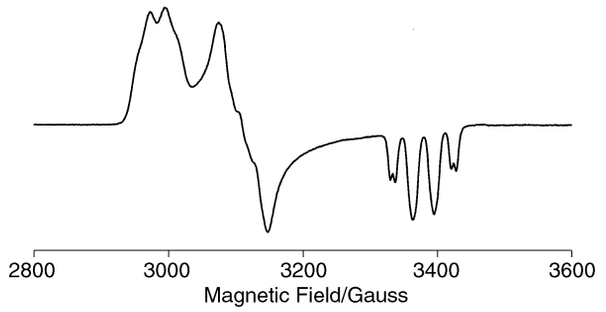

Fig. 12 The anisotropic ESR spectrum of $[Rh(CO)\{P(C_6H_4Me\text{-}m)_3\}Tp']^+$ $\mathbf{6}^+$ at 120 K in CH_2Cl_2–1,2-dichloroethane (1 : 1).

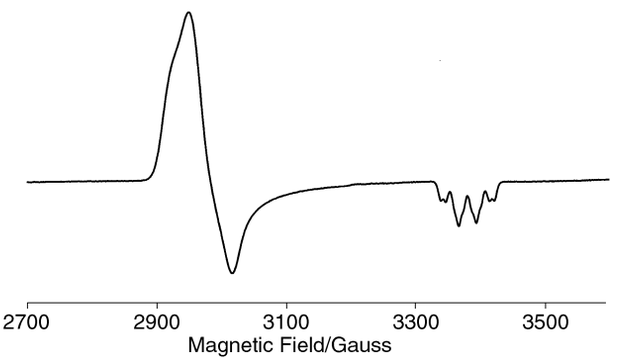

Fig. 13 The anisotropic ESR spectrum of $[Rh(PPh_3)_2Tp']^+$ $\mathbf{8}^+$ at 100 K in CH_2Cl_2–1,2-dichloroethane (1 : 1).

and ^{31}P) for the carbonyl phosphine and bis(phosphine) complexes, or one $I = 1$ nucleus (^{14}N) and one $I = 1/2$ nucleus (^{103}Rh) for $[Rh(CO)_2Tp']^+$ $\mathbf{1}^+$ and $[Rh(CO)\{P(NMe_2)_3\}Tp']^+$ $\mathbf{4}^+$. The central feature consists of a triplet for $[Rh(CO)_2Tp']^+$ $\mathbf{1}^+$ and $[Rh(CO)LTp']^+$ {L = PPh_3 $\mathbf{2}^+$ or $P(C_6H_4Me\text{-}p)_3$ $\mathbf{5}^+$} due to coupling to ^{14}N. However, in the spectra of $[Rh(CO)LTp']^+$ {L = $P(NMe_2)_3$ $\mathbf{4}^+$ or $P(C_6H_4Me\text{-}m)_3$ $\mathbf{6}^+$} there is additional coupling to an $I = 1/2$ nucleus, probably ^{103}Rh. The low-field feature showed coupling to $I = 1$ and $I = 1/2$ nuclei for $[Rh(CO)LTp']^+$ {L = CO $\mathbf{1}^+$, PPh_3 $\mathbf{2}^+$, $P(NMe_2)_3$ $\mathbf{4}^+$, $P(C_6H_4\text{-}Me\text{-}p)_3$ $\mathbf{5}^+$ or $P(C_6H_4Me\text{-}m)_3$ $\mathbf{6}^+$}.

The spectra are almost textbook examples of the expectations for a square pyramidal low-spin d^7 complex, necessarily with d_{z^2} as the metal contribution to the SOMO (and consistent with the solid state structures of $\mathbf{2}^+$ and $\mathbf{4}^+$). This conclusion is based on the fact that (i) the smallest g component is close to 2, and (ii) coupling to only one ^{14}N atom is observed and that coupling is unusually large.

One unexpected observation, however, is the failure to see coupling to both phosphorus nuclei in $[Rh(PPh_3)_2L']^+$ {L′ = Tp′ $\mathbf{8}^+$, Tp $\mathbf{9}^+$ or $B(pz)_4$ $\mathbf{10}^+$} and $[Rh(dppe)Tp']^+$ $\mathbf{11}^+$. However, the solid state structure of $\mathbf{8}^+$ is significantly distorted from an ideal square pyramid with one phosphorus atom tilted out of the square plane (N_{axial}–Rh–P 90 and 103°); if a similar geometry is adopted in solution, the inequivalence of the phosphorus atoms may explain the missing coupling.

Another unexpected observation is the discrepancy between the isotropic g value, g_{iso}, and the average of the three components from the frozen solution spectra, g_{ave}. The difference between g_{iso} and g_{ave} is always positive with a value between 0.003 and 0.012 for the carbonyl phosphine complexes and between 0.013 and 0.023 for the bis(phosphine) or ditertiary phosphine complexes. This difference may indicate a significant change in the electronic structure of the metal(II) complexes with temperature, possibly due to some departure from square pyramidal geometry leading to admixture of other metal d-orbital character to the SOMO. Further detailed studies of the variable temperature spectra are in progress.

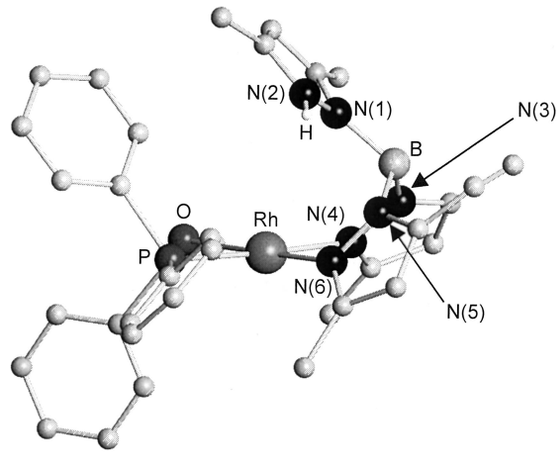

Fig. 14 The molecular structure of the cation $[Rh(CO)(PPh_3)(HTp')]^+$ in $[Rh(CO)(PPh_3)(HTp')][BF_4]$·thf **12**·thf. Most hydrogen atoms have been omitted for clarity.

The protonation of [Rh(CO)LTp′] and [RhL_2Tp']

As noted above, the chemical oxidation of $[Rh(CO)_2Tp']$ **1** results in the formation of the κ^2-rhodium(I) *N*-protonated complex $[Rh(CO)_2(HTp')][BF_4]$.[6,33] In order to confirm that similar species result from the decomposition of the rhodium(II) cations $[Rh(CO)(PR_3)Tp']^+$ the representative complex $[Rh(CO)(PPh_3)(HTp')][BF_4]$ **12** has been prepared by direct protonation of **2** and fully characterised. The reaction of $[Rh(CO)(PPh_3)Tp']$ with HBF_4 in diethyl ether resulted in the formation of a yellow precipitate which was characterised by elemental analysis, IR and NMR spectroscopy (Tables 1 and 2), and X-ray crystallography as the *N*-protonated complex $[Rh(CO)(PPh_3)(HTp')][BF_4]$ **12**. {Complex **12** also results from the reaction between $[Rh(CO)_2(HTp')][BF_4]$ and PPh_3 in CH_2Cl_2, carbonyl substitution being much faster than for the neutral complex $[Rh(CO)_2Tp']$ **1**.} Similar species were generated by protonating $[Rh(CO)LTp']$ {L = $P(C_6H_4Me\text{-}p)_3$, $P(C_6H_4\text{-}Me\text{-}m)_3$, PCy_3, $P(NMe_2)_3$ or $P(OPh)_3$} but identified only by their IR carbonyl bands, at 1986, 1988, 1974, 1983 and 2022 cm^{-1} respectively.

Although the *N*-protonated complexes are cationic, rhodium remains in oxidation state I so that ν(CO) is only 10–15 cm^{-1} higher than that of the neutral complexes {*cf.* the shift of *ca.* 90 cm^{-1} for oxidation to Rh^{II}}. Values of ν(BH) for **12**, *etc.* are approximately 40 cm^{-1} higher than those of the neutral complexes **2**–**4** and **6**. As noted above, the change from a neutral to a cationic complex leads to an increase in ν(BH) of approximately 20 cm^{-1} if the bonding mode (κ^2 or κ^3) of the pyrazolylborate ligand is unchanged. Thus, it appears that an additional increase in ν(BH) (*ca.* 20 cm^{-1}) accompanies *N*-protonation of the hydrotris(pyrazolyl)borate ligand.

Crystals of $[Rh(CO)(PPh_3)(HTp')][BF_4]$·thf **12** were grown by allowing a concentrated thf solution of the complex to diffuse slowly into *n*-hexane at −10 °C. The structure of **12**, shown in Fig. 14 with selected bond lengths and angles collected in Table 3, is very similar to that of neutral $[Rh(CO)(PPh_3)Tp']$ **2**, with square planar geometry at rhodium and the *N*-protonated pyrazolyl ring positioned as parallel as possible with respect to the square plane about rhodium. A similar geometry is seen for the dicarbonyl analogue of the cation of **12**, $[Rh(CO)_2(HTp')]^+$.[33] The structure of **12** is consistent with its NMR spectra (Table 2) in that all three pyrazolyl rings are inequivalent (*cf.* the fluxionality of **2**) fast interconversion being prevented by protonation of the unco-ordinated pyrazolyl ring.

N-Protonation of complex **1** is reversed by reduction. Thus, the CV of $[Rh(CO)_2(HTp')][BF_4]$ shows an irreversible reduction wave at *ca.* −1.2 V and reduction with $[Co(\eta\text{-}C_5H_5)_2]$ regenerates neutral $[Rh(CO)_2Tp']$ **1**.

Conclusion

Two series of rhodium(I) complexes, namely [Rh(CO)LTp′] (L = phosphine or phosphite) and [Rh(PPh_3)$_2$L′] {L′ = Tp′, Tp or B(pz)$_4$} or [Rh(dppe)Tp′], have been synthesized. IR spectroscopy and single crystal X-ray studies have shown ligand dependent structures; most adopt a κ^2 square planar form with the third, unbound pyrazolyl ring orientated pseudo-parallel to the rhodium co-ordination plane. However, [Rh(CO){P(OPh)$_3$}Tp′] **7** has a distorted square pyramidal structure with the rhodium essentially in the plane of the basal ligands and with a very long Rh–apical ligand distance. Though described as κ^3 bound, **7** differs from 'conventional' κ^3 rhodium(I) complexes which have trigonal pyramidal geometry with a short, third, Rh–N bond to the hydrotris(pyrazolyl) borate ligand.

The complexes [Rh(CO)LTp′] show fluxional behaviour in which the three pyrazolyl rings become equivalent at higher temperatures by processes which involve both square pyramidal and trigonal bipyramidal intermediates.

One-electron oxidation of the rhodium(I) complexes, at platinum or glassy carbon electrodes or with chemical one-electron oxidants, gives monocationic rhodium(II) analogues such as [Rh(CO)LTp′]$^+$ and [Rh(dppe)Tp′]$^+$ which have square pyramidal structures with κ^3-bound pyrazolyl ligands. The results of X-ray structural and ESR spectroscopic studies are consistent with population of a Rh–N_{axial} σ* orbital on reduction of the rhodium(II) cations.

Experimental

The preparation, purification and reactions of the complexes described were carried out under an atmosphere of dry nitrogen using dried, distilled and deoxygenated solvents; reactions were monitored by IR spectroscopy where necessary. Thermal substitution reactions of [Rh(CO)$_2$Tp′] were carried out in the absence of light. Unless stated otherwise complexes (i) were purified by dissolution in CH_2Cl_2, filtration of the solution through Celite, addition of *n*-hexane to the filtrate and reduction of the volume of the mixture *in vacuo* to induce precipitation, and (ii) are stable under nitrogen and dissolve in polar solvents such as CH_2Cl_2 and thf. Most complexes give moderately air-stable solutions; [Rh(dppe)Tp′]^z (z = 0 or 1), [Rh(PPh_3)$_2$L′]^z {z = 0 or 1; L′ = Tp or B(pz)$_4$} are less stable in solution. The compounds [{Rh(μ-Cl)(PPh_3)$_2$}$_2$],[36] [{Rh(μ-Cl)(dppe)}$_2$],[37] KTp′, KTp, K[B(pz)$_4$],[38] [Rh(CO)$_2$Tp′],[10] [Fe(η-C_5H_5)$_2$][PF_6], [Fe(η-C_5H_5)(η-C_5H_4COMe)][PF_6] and [Co(η-C_5H_5)$_2$][39] were prepared by published methods.

IR spectra were recorded on a Nicolet 5ZDX FT spectrometer and UV-visible spectra on a Perkin-Elmer Lambda 2 UV/VIS spectrometer. X-Band ESR spectra were obtained on a Bruker 300ESP spectrometer equipped with a Bruker variable temperature accessory and a Hewlett-Packard 5350B microwave frequency counter. The field calibration was checked by measuring the resonance of the diphenylpicrylhydrazyl (dpph) radical before each series of spectra. NMR spectra were recorded on JEOL GX270, GX400 and λ300 spectrometers with $SiMe_4$ as an internal standard. All spectrometers operated in the Fourier transform mode, with field stability maintained by an external lock system. Electrochemical studies were carried out using an EG&G model 273 potentiostat in conjunction with a three-electrode cell. For cyclic voltammetry the auxiliary electrode was a platinum wire and the working electrode a glassy-carbon (3.0 mm diameter) or platinum (1.0 mm diameter) disc. The reference was an aqueous saturated calomel electrode separated from the test solution by a fine-porosity frit and an agar bridge saturated with KCl. Solutions were 0.1×10^{-3} or 5×10^{-4} mol dm^{-3} in the test compound and 0.1 mol dm^{-3} in [NBu_4][PF_6] as the supporting electrolyte. Potentials are quoted *vs.* the [Fe(η-C_5H_5)$_2$]$^+$–[Fe(η-C_5H_5)$_2$] couple ($E^{\circ\prime}$ = 0.0 V) as the internal standard. Peak-to-peak separations {*i.e.* $(E_p)_{ox} - (E_p)_{red}$} were compared with those for an appropriate internal standard ([Fe(η-C_5H_5)$_2$] or [Fe(η-C_5Me_5)$_2$]) under conditions where the concentrations of the sample and standard were adjusted to give waves with the same peak currents. Microanalyses were carried out by the staff of the Microanalytical Service of the School of Chemistry, University of Bristol.

Syntheses

[Rh(CO)(PPh_3)Tp′] 2. A mixture of [Rh(CO)$_2$Tp′] **1** (1.0 g, 2.19 mmol) and PPh_3 (575 mg, 2.19 mmol) in *n*-hexane (250 cm^3) was heated under reflux for 24 h before being cooled to −10 °C to precipitate a grey-yellow solid. A CH_2Cl_2 (40 cm^3) solution of the solid was filtered through Celite and then concentrated *in vacuo* before *n*-hexane was added to give a bright yellow powder which was dried *in vacuo*, yield 1.0 g (67%).

[Rh(CO)(PCy_3)Tp′] 3. A suspension of [Rh(CO)$_2$Tp′] **1** (0.50 g, 1.10 mmol) and PCy_3 (0.34 g, 1.21 mmol) in *n*-hexane (250 cm^3) was heated under reflux for 4 h. The resulting solution was evaporated to dryness *in vacuo* to give a yellow solid which was dissolved in the minimum volume of toluene and chromatographed on alumina. Impurities were washed from the column with diethyl ether–*n*-hexane (1 : 9) and the product eluted with diethyl ether. The resulting pale yellow solution was evaporated to dryness *in vacuo* to give a pale yellow solid which was dried *in vacuo* for 3 d, yield 325 mg (42%).

[Rh(CO){P(NMe_2)$_3$}Tp′] 4. A solution of [Rh(CO)$_2$Tp′] **1** (0.30 g, 0.66 mmol) and P(NMe_2)$_3$ (0.120 cm^3, 0.66 mmol) in toluene (70 cm^3) was stirred for 2 h. The resulting bright yellow solution was evaporated to dryness *in vacuo* to give a yellow solid which was dissolved in hot *n*-hexane (35 cm^3), filtered through Celite and then stored at −10 °C for 5 d to yield 190 mg of large yellow crystals. The mother liquors were evaporated to lower volume *in vacuo* and stored at −10 °C for 5 d to give another 60 mg of crystals. Total yield 250 mg (64%).

[Rh(CO){P(C_6H_4Me-*p*)$_3$}Tp′] 5. A solution of [Rh(CO)$_2$Tp′] **1** (0.20 g, 0.44 mmol) and P(C_6H_4Me-*p*)$_3$ (134 mg, 438 μmol) in toluene (50 cm^3) was stirred for 24 h, and then evaporated to dryness *in vacuo* to leave a yellow oil. The oil was dissolved in diethyl ether, layered with *n*-hexane and stored at −10 °C to give a bright yellow precipitate which was dried *in vacuo*, yield 138 mg (43%).

[Rh(CO){P(C_6H_4Me-*m*)$_3$}Tp′] 6. A solution of [Rh(CO)$_2$Tp′] **1** (0.20 g, 0.44 mmol) and P(C_6H_4Me-*m*)$_3$ (134 mg, 438 μmol) in toluene (50 cm^3) was stirred for 24 h, and then evaporated to dryness *in vacuo* to leave a yellow oil. The oil was dissolved in hot *n*-hexane and cooled to −10 °C to give a dull green-yellow solid which was redissolved in hot *n*-hexane and cooled to −10 °C to yield green-yellow crystals which were dried *in vacuo*, yield 144 mg (45%).

[Rh(CO){P(OPh_3)$_3$}Tp′] 7. A solution of [Rh(CO)$_2$Tp′] **1** (295 mg, 0.65 mmol) and P(OPh_3)$_3$ (0.17 cm^3, 0.65 mmol) in toluene (60 cm^3) was heated at 50 °C for 24 h and evaporated to dryness *in vacuo*. The resulting yellow oil was dissolved in hot *n*-hexane (80 cm^3) and then filtered. The filtrate was cooled to −10 °C to give yellow-orange crystals, yield 154 mg (32%).

[Rh(PPh_3)$_2$Tp′] 8. A suspension of [{Rh(μ-Cl)(PPh_3)$_2$}$_2$] (200 mg, 0.15 mmol) and KTp′ (101 mg, 0.30 mmol) in thf (50 cm^3) was stirred for 3 h and then evaporated to dryness *in vacuo*. The

Table 5 Crystal and refinement data for [Rh(CO)(PPh_3)Tp′] **2**, [Rh(CO)(PCy_3)Tp′] **3**, [Rh(CO){$P(NMe_2)_3$}Tp′] **4**, [Rh(CO){$P(C_6H_4Me\text{-}m)_3$}Tp′] **6**, [Rh(CO){$P(OPh)_3$}Tp′] **7**, [Rh(PPh_3)$_2$Tp′]·C_6H_{14} **8**·C_6H_{14}, [Rh(CO)(PPh_3)(HTp′)][BF_4]·thf **12**·thf, [Rh(CO)(PPh_3)Tp′][PF_6]·CH_2Cl_2 **2**$^+$[PF_6]$^-$·CH_2Cl_2 and [Rh(PPh_3)$_2$Tp′]X·3CH_2ClCH_2Cl **8**$^+$ X^-·3CH_2ClCH_2Cl (X^- = [PF_6]$^-$ or [BF_4]$^-$)[a]

Compound	**2**	**3**	**4**	**6**	**7**	**8**·C_6H_{14}	**12**·thf	**2**$^+$[PF_6]$^-$·CH_2Cl_2	**8**$^+$[PF_6]$^-$·3CH_2ClCH_2Cl	**8**$^+$ [BF_4]$^-$·3CH_2ClCH_2Cl
Formula	$C_{34}H_{38}BN_6OPRh$	$C_{34}H_{55}BN_6OPRh$	$C_{22}H_{40}BN_9OPRh$	$C_{37}H_{43}BN_6OPRh$	$C_{34}H_{37}BN_6O_4PRh$	$C_{54}H_{52}BN_6P_2Rh$	$C_{38}H_{46}B_2F_4N_6O_2PRh$	$C_{35}H_{39}BCl_2F_6N_6OP_2Rh$	$C_{57}H_{64}BCl_6F_6N_6P_3Rh$	$C_{57}H_{60}B_2Cl_6F_4N_6P_2Rh$
Formula weight	691.39	708.53	591.32	732.46	738.39	960.68	850.31	920.28	1366.47	1304.28
Crystal system	Monoclinic	Monoclinic	Triclinic	Triclinic	Triclinic	Monoclinic	Triclinic	Monoclinic	Triclinic	Triclinic
Space group (no.)	$P2_1/n$ (no. 14)	$P2_1/n$ (no. 14)	$P\bar{1}$ (no. 2)	$P\bar{1}$ (no. 2)	$P\bar{1}$ (no. 2)	$P2_1/n$ (no. 14)	$P\bar{1}$ (no. 2)	$P2_1/n$ (no. 14)	$P\bar{1}$ (no. 2)	$P\bar{1}$ (no. 2)
a/Å	9.428(3)	12.567(4)	9.287(3)	10.8099(17)	10.4975(17)	11.4436(11)	9.6364(12)	10.6665(19)	10.630(3)	10.6624(15)
b/Å	16.510(4)	22.521(8)	10.529(3)	12.0504(12)	12.1867(17)	18.7695(18)	10.507(2)	15.0904(23)	17.590(4)	17.463(2)
c/Å	20.735(5)	12.931(3)	16.589(4)	13.737(3)	13.7717(15)	23.137(3)	20.417(4)	25.2607(35)	17.957(3)	17.664(4)
α/°	97.73(3)	102.71(2)	72.50(2)	96.536(12)	87.865(8)		75.132(9)		95.33(2)	93.214(12)
β/°			77.36(2)	93.879(12)	87.751(9)	91.323(8)	87.82(2)	90.781(14)	102.693(19)	103.270(11)
γ/°			69.48(3)	92.424(5)	78.014(12)		86.56(2)		107.102(16)	107.329(12)
V/Å^3	3198(2)	3570(2)	1437.2(7)	1771.4(5)	1721.3(4)	4968(1)	1993.8(6)	4065.6(2)	3085.7(12)	3028.4(9)
Z	4	4	2	2	2	4	2	4	2	2
μ/mm^{-1}	0.622	0.558	0.681	0.566	0.589	0.450	0.528	0.694	0.675	0.654
Reflections collected	14466	34555	12462	15270	17504	31048	20537	19030	20832	25610
Independent reflections	5582	8155	5032	6205	7766	11340	9047	7130	10676	10566
Final $R1$ [$I > 2\sigma(I)$]	0.0688	0.0674	0.0542	0.0277	0.0288	0.0305	0.0497	0.0331	0.0919	0.0655

[a] The crystal structure analysis of **4**$^+$ [PF_6]$^-$·CH_2ClCH_2Cl·0.5H_2O was severely hampered by twinning. An incomplete determination was possible, yielding the following crystal data: $C_{24}H_{44}BCl_2F_6N_9O_{1.5}P_2Rh$, M = 843.24, orthorhombic, space group $Pca2_1$ (no. 29), a = 24.390(10), b = 13.330(4), c = 22.563(10) Å, U = 7336(5) Å^3, Z = 8, μ(Mo-Kα) = 0.764, $R1$ = 0.1447, 9746 reflections.

resulting oily orange solid was dissolved in diethyl ether (40 cm^3), filtered through Celite, and concentrated *in vacuo* before *n*-hexane was added to precipitate a bright yellow solid which was dried *in vacuo*, yield 135 mg (48%).

The complexes $[Rh(PPh_3)_2Tp]$ **9** and $[Rh(PPh_3)_2\{B(pz)_4\}]$ **10** were prepared similarly, but only required stirring for 1 h (under N_2) or 45 min (under Ar) respectively.

[Rh(dppe)Tp′] 11. A solution of $[\{Rh(\mu\text{-}Cl)(dppe)\}_2]$ (300 mg, 0.278 mmol) and KTp′ (188 mg, 0.56 mmol) in thf (40 cm^3) was stirred for 4 h and then evaporated to dryness *in vacuo*. The resulting solid was dissolved in diethyl ether, filtered through Celite and concentrated *in vacuo* before *n*-hexane was added to precipitate a bright yellow powder which was dried *in vacuo*, yield 180 mg (40%).

[Rh(CO)(PPh$_3$)(HTp′)][BF$_4$] 12. Solid [Rh(CO)(PPh_3)Tp′] **2** (100 mg, 0.15 mmol) was added to a stirred solution of $HBF_4{\cdot}OEt_2$ (0.20 cm^3, 0.15 mmol) in diethyl ether (40 cm^3). After 10 min, the pale yellow mother liquors were removed to leave a pale yellow precipitate which was purified using CH_2Cl_2–*n*-hexane, yield 67 mg (60%).

[Rh(CO)(PPh$_3$)Tp′][PF$_6$]·CH$_2$Cl$_2$ 2$^+$[PF$_6$]$^-$·CH$_2$Cl$_2$. Solid $[Fe(\eta\text{-}C_5H_5)_2][PF_6]$ (0.23 g, 0.69 mmol) was added to a CH_2Cl_2 (180 cm^3) solution of [Rh(CO)(PPh_3)Tp′] **2** (0.50 g, 0.72 mmol) at 0 °C. After 1 h the green solution was filtered through Celite and concentrated *in vacuo* before *n*-hexane was added to precipitate a dark green solid which was washed with *n*-hexane and dried *in vacuo*, yield 455 mg (72%).

The complexes $[Rh(CO)\{P(NMe_2)_3\}Tp'][PF_6]$ $\mathbf{4}^+[PF_6]^-$ and $[Rh(PPh_3)_2Tp'][X]$ ($X^- = [PF_6]^-$ or $[BF_4]^-$) $\mathbf{8}^+X^-$ were prepared similarly as purple solids after stirring for 1 h, 10 min and 40 min respectively.

[Rh(CO){P(C$_6$H$_4$Me-*p*)$_3$}Tp′][PF$_6$]·0.7CH$_2$Cl$_2$ 5$^+$[PF$_6$]$^-$·0.7CH$_2$Cl$_2$. Solid $[Fe(\eta\text{-}C_5H_5)_2][PF_6]$ (42 mg, 0.12 mmol) was added to a CH_2Cl_2 (15 cm^3) solution of $[Rh(CO)\{P(C_6H_4\text{-}Me\text{-}p)_3\}Tp']$ **5** (115 mg, 0.16 mmol) at 0 °C. After 1 h the solution was evaporated to dryness *in vacuo* to leave a green oil which was dissolved in $CHCl_3$ (10 cm^3), filtered through Celite and evaporated to dryness *in vacuo*. Purification using thf–*n*-hexane (twice) gave a dark green solid which was washed with *n*-hexane and dried *in vacuo*, yield 63 mg (53%).

Grey-green $[Rh(CO)\{P(C_6H_4Me\text{-}m)_3\}Tp'][PF_6]{\cdot}0.5CH_2Cl_2$ $\mathbf{6}^+[PF_6]^-{\cdot}0.5CH_2Cl_2$ was prepared similarly but washed with diethyl ether instead of *n*-hexane and dried *in vacuo* for 3 d.

[Rh(PPh$_3$)$_2$Tp][PF$_6$]·0.5CH$_2$Cl$_2$ 9$^+$[PF$_6$]$^-$·0.5CH$_2$Cl$_2$. Solid $[Fe(\eta\text{-}C_5H_5)_2][PF_6]$ (35 mg, 0.11 mmol) was added to a CH_2Cl_2 (15 cm^3) solution of $[Rh(PPh_3)_2Tp]$ **9** (100 mg, 0.12 mmol) at 0 °C. After 1 h *n*-hexane was added to the orange-brown solution to produce a purple-brown oil which was washed with *n*-hexane. The oil was dissolved in CH_2Cl_2 (10 cm^3) to give a purple-brown solution to which diethyl ether was added. The volume of the mixture was reduced *in vacuo* until an oily solid began to form. *n*-Hexane was then added to the well stirred mixture to give a voluminous purple precipitate. The yellow mother liquors were removed and the very air-sensitive pale purple solid was dried *in vacuo* and stored in a glove-box under argon, yield 82 mg (75%).

[Rh(dppe)Tp′][PF$_6$] 11$^+$[PF$_6$]$^-$. Solid $[Fe(\eta\text{-}C_5H_5)_2][PF_6]$ (37.5 mg, 0.11 mmol) was added to a CH_2Cl_2 (15 cm^3) solution of [Rh(dppe)Tp′] **11** (100 mg, 0.13 mmol) at 0 °C. After 1 h the yellow-brown solution was filtered through Celite and concentrated *in vacuo* before *n*-hexane was added to give a green-brown solid. The solid was washed with *n*-hexane and dried *in vacuo* for 3 d to give the olive green product, yield 74 mg (69%).

Generation of [Rh(CO)LTp′]$^+$ {L = CO (1$^+$), PPh$_3$ (2$^+$), PCy$_3$ (3$^+$), P(NMe$_2$)$_3$ (4$^+$), P(C$_6$H$_4$Me-*p*)$_3$ (5$^+$), P(C$_6$H$_4$Me-*m*)$_3$ (6$^+$) or P(OPh)$_3$ (7$^+$)}, [Rh(PPh$_3$)$_2$L′]$^+$ {L′ = Tp′ (8$^+$), Tp (9$^+$) or B(pz)$_4$ (10$^+$)} and [Rh(dppe)Tp′] 11$^+$ at low temperature for ESR spectroscopy. The neutral poly(pyrazolyl)borate complex was dissolved in 1 : 1 CH_2Cl_2–CH_2ClCH_2Cl in a silica ESR tube. The mixture was degassed (three freeze–pump–thaw cycles) and then $[Fe(\eta\text{-}C_5H_5)_2][PF_6]$ or $[Fe(\eta\text{-}C_5H_5)(\eta\text{-}C_5H_4COMe)][PF_6]$ was added to the frozen solution at 77 K. The tube was then evacuated, filled with nitrogen and transferred to the cavity of the ESR spectrometer at 200 K. The temperature was raised to 220 K to allow mixing of the reagents before cooling to between 100 and 120 K to record the anisotropic spectrum. If a well resolved spectrum was not obtained, the tube was removed from the cavity of the spectrometer, and the contents annealed and then refrozen. The temperature was then raised in approximately 20 K increments until a well resolved isotropic spectrum was obtained or the signal disappeared. In several cases, after obtaining the isotropic spectrum the temperature was lowered to re-record the anisotropic spectrum.

Crystal structure determinations of complexes 2–4, 6, 7, 8·C$_6$H$_{14}$, 12·thf, 2$^+$[PF$_6$]$^-$·CH$_2$Cl$_2$, 4$^+$[PF$_6$]$^-$·CH$_2$ClCH$_2$Cl·0.5H$_2$O and 8$^+$X$^-$·3CH$_2$ClCH$_2$Cl (X$^-$ = [PF$_6$]$^-$ or [BF$_4$]$^-$). Crystals suitable for X-ray diffraction study were grown as follows: **2**, slowly cooling a hot *n*-hexane solution of the complex to room temperature; **3**, slowly evaporating an *n*-pentane solution of the complex under N_2 at −10 °C; **4**, **6**, **7** and **8**·C_6H_{14}, slowly cooling a hot *n*-hexane solution of the complex to −10 °C; **12**·thf, slow diffusion of a concentrated thf solution of the complex into *n*-hexane at −10 °C; $\mathbf{2}^+[PF_6]^-{\cdot}CH_2Cl_2$, slow diffusion of a concentrated CH_2Cl_2 solution of the complex into *n*-hexane at −10 °C; $\mathbf{4}^+[PF_6]^-{\cdot}CH_2ClCH_2Cl{\cdot}0.5H_2O$ and $\mathbf{8}^+X^-{\cdot}3CH_2ClCH_2Cl$ ($X^- = [PF_6]^-$ or $[BF_4]^-$), slow diffusion of a concentrated 1,2-dichloroethane solution of the complex into *n*-hexane at −10 °C. All X-ray diffraction measurements were made at 173 K. Many of the other details of the structure analyses are presented in Table 5.

The structure of complex $\mathbf{2}^+[PF_6]^-{\cdot}CH_2Cl_2$ contains a disordered dichloromethane with chlorines populating two sites, occupancy 77(1) : 23(1). The *n*-hexane in **8**·C_6H_{14} is disordered as are two of the solvent molecules in both $\mathbf{8}^+X^-{\cdot}3CH_2ClCH_2Cl$, $X^- = [PF_6]^-$ or $[BF_4]^-$. Complex **4** also shows disorder, with the carbonyl, the methyl group C(6) and the NMe_2 groups all populating two sites with a 50% occupancy. The structure of $\mathbf{4}^+[PF_6]^-{\cdot}CH_2ClCH_2Cl{\cdot}0.5H_2O$ contains two independent formula units in the asymmetric unit and what appears to be a partially occupied water site. The data for this structure determination were very poor and weak and the structure is inversion twinned; the analysis is therefore incomplete (see footnote to Table 5).

CCDC reference number 186/2314.

See http://www.rsc.org/suppdata/dt/b0/b008131k/ for crystallographic files in .cif format.

Acknowledgements

We thank the EPSRC for Research Studentships (to D. J. H. E, O. D. H. and M. J. Q.).

References

1 U. E. Bucher, A. Currao, R. Nesper, H. Ruegger, L. M. Venanzi and E. Younger, *Inorg. Chem.*, 1995, **34**, 66.
2 M. Akita, K. Ohta, Y. Takahashi, S. Hikichi and Y. Moro-oka, *Organometallics*, 1997, **16**, 4121.
3 N. Kitajima and W. B. Tolman, *Prog. Inorg. Chem.*, 1995, **43**, 419.
4 D. Sanz, D. M. Santa María, R. M. Claramunt, M. Cano, J. V. Heras, J. A. Campo, F. A. Ruíz, E. Pinilla and A. Monge, *J. Organomet. Chem.*, 1996, **526**, 341.

5 A. A. Purwoko, S. D. Tibensky and A. J. Lees, *Inorg. Chem.*, 1996, **35**, 7049.
6 A. A. Purwoko and A. J. Lees, *Inorg. Chem.*, 1996, **35**, 675.
7 C. K. Ghosh and W. A. G. Graham, *J. Am. Chem. Soc.*, 1987, **109**, 4726.
8 S. E. Bromberg, H. Yang, M. C. Asplund, T. Lian, B. K. McNamara, K. T. Kotz, J. S. Yeston, M. Wilkens, H. Frei, R. G. Bergman and C. B. Harris, *Science*, 1997, **278**, 260; J. S. Yeston, B. K. McNamara, R. G. Bergman and C. B. Moore, *Organometallics*, 2000, **19**, 3442.
9 N. G. Connelly, D. J. H. Emslie, B. Metz, A. G. Orpen and M. J. Quayle, *Chem. Commun.*, 1996, 2289.
10 S. May, P. Reinsalu and J. Powell, *Inorg. Chem.*, 1980, **19**, 1582.
11 V. Chauby, C. S. Le Berre, P. Kalck, J.-C. Daran and G. Commenges, *Inorg. Chem.*, 1996, **35**, 6354.
12 M. Paneque, S. Sirol, M. Trujillo, E. Gutierrez-Puebla, M. A. Monge and E. Carmona, *Angew. Chem., Int. Ed.*, 2000, **39**, 218.
13 F. Malbosc, P. Kalck, J.-C. Daran and M. Etienne, *J. Chem. Soc., Dalton Trans.*, 1999, 271.
14 A. F. Hill, A. J. P. White, D. J. Williams and J. D. E. T. Wilton-Ely, *Organometallics*, 1998, **17**, 3152.
15 M. Akita, M. Hashimoto, S. Hikichi and Y. Moro-oka, *Organometallics*, 2000, **19**, 3747.
16 E. Del Ministro, O. Renn, H. Ruegger, L. M. Venanzi, U. Burckhardt and V. Gramlich, *Inorg. Chim. Acta*, 1995, **240**, 631.
17 T. O. Northcutt, R. J. Lachicotte and W. D. Jones, *Organometallics*, 1998, **17**, 5148.
18 C. A. Tolman, *Chem. Rev.*, 1977, **77**, 313.
19 A. G. Orpen, L. Brammer, F. H. Allen, O. Kennard, D. G. Watson and R. Taylor, *J. Chem. Soc., Dalton Trans.*, 1989, S1.
20 J. Emsley, *The Elements*, Clarendon Press, Oxford, 2nd edn., 1991.
21 T. P. E. Auf der Heyde and H.-B. Burgi, *Inorg. Chem.*, 1989, **28**, 3960; T. P. E. Auf der Heyde and H.-B. Burgi, *Inorg. Chem.*, 1989, **28**, 3970; T. P. E. Auf der Heyde and H.-B. Burgi, *Inorg. Chem.*, 1989, **28**, 3982.
22 A. L. Rheingold, R. L. Ostrander, B. S. Haggerty and S. Trofimenko, *Inorg. Chem.*, 1994, **33**, 3666.
23 D. D. Wick, T. O. Northcutt, R. J. Lachicotte and W. D. Jones, *Organometallics*, 1998, **17**, 4484.
24 T. A. Albright, J. K Burdett and M. H. Whangbo, *Orbital Interactions in Chemistry*, Wiley-Interscience, New York, 1985.
25 W. E. Geiger, B. Yeomans, N. G. Connelly and D. J. H. Emslie, unpublished results.
26 D. G. DeWit, *Coord. Chem. Rev.*, 1996, **147**, 209.
27 M. P. Garcia, M. V. Gimenez, A. Cuesta, C. Siruana, L. A. Oro, F. J. Lahoz, J. A. Lopez and M. P. Catalan, *Organometallics*, 1997, **16**, 1026.
28 D. Menglet, A. M. Bond, K. Coutinho, R. S. Dickson, G. G. Lazarev, S. A. Olsen and J. R. Pilbrow, *J. Am. Chem. Soc.*, 1998, **120**, 2086.
29 P. Paul, B. Tyagi, A. K. Bilakhiya, M. M. Bhadbhade and E. Suresh, *J. Chem. Soc., Dalton Trans.*, 1999, 2009.
30 S. Trofimenko, *Chem. Rev.*, 1993, **93**, 943.
31 N. G. Connelly, A. R. Lucy, J. D. Payne, A. M. R. Galas and W. E. Geiger, *J. Chem. Soc., Dalton Trans.*, 1983, 1879.
32 D. M. Tellers, S. J. Skoog, R. G. Bergman, T. B. Gunnoe and W. D. Harman, *Organometallics*, 2000, **19**, 2428.
33 R. G. Ball, C. K. Ghosh, J. K. Hoyano, A. D. McMaster and W. A. G. Graham, *J. Chem. Soc., Chem. Commun.*, 1989, 341.
34 D. J. Harding, Ph.D. Thesis, University of Bristol, 2000.
35 N. G. Connelly, D. J. H. Emslie, O. D. Hayward, A. G. Orpen and M. J. Quayle, *J. Chem. Soc., Dalton Trans.*, 2001, DOI: 10.1039/b010061g.
36 J. A. Osborn and G. Wilkinson, *Inorg. Synth.*, 1990, **28**, 77.
37 P. Albano, M. Aresta and M. Manassero, *Inorg. Chem.*, 1980, **19**, 1069.
38 S. Trofimenko, *Inorg. Synth.*, 1970, **12**, 99.
39 N. G. Connelly and W. E. Geiger, *Chem. Rev.*, 1996, **96**, 877.